Structural basis for collagen recognition by the *Streptococcus pyogenes* M3 protein and its involvement in biofilm

Marta Wojnowska[1*#], Takeaki Wajima[2*†], Tamas Yelland[3€], Hannes Ludewig[1¶], Robert M. Hagan[1], Olivia F. McCurry[1], Grant Watt[1], Samir W. Hamaia[4], Dominique Bihan[4], Jean-Daniel Malcor[4&], Arkadiusz Bonna[4±], Helena Bergsten[2], Laura M. Palma Medina[2], Mattias Svensson[2], Oddvar Oppegaard[5], Steinar Skrede[5], Per Arnell[6], Ole Hyldegaard[7], Richard W. Farndale[4±], Anna Norrby-Teglund[2§], Ulrich Schwarz-Linek[1§]

[1]Biomedical Sciences Research Complex, University of St Andrews, North Haugh, St Andrews, KY16 9ST, UK

[2]Center for Infectious Medicine, Karolinska Institutet, Karolinska University Hospital Huddinge, Sweden

[3]CRUK Beatson Institute, Glasgow G61 1BD, UK

[4]Department of Biochemistry, University of Cambridge, Downing Site, Cambridge, CB2 1QW, UK

[5]Department of Medicine, Haukeland University Hospital, Bergen, Norway, Department of Clinical Science, University of Bergen, Norway

[6]Department of Anesthesiology and Intensive Care Medicine, Sahlgrenska University Hospital, Gothenburg, Sweden

[7]Department of Anesthesiology, Hyperbaric Medicine Center, Head and Orthopedic Center, Copenhagen University Hospital, Rigshospitalet, Copenhagen, Denmark and Department of Clinical Medicine, University of Copenhagen

* equal contribution first authors

[#] current address: Department of Biochemistry, University of Cambridge, Tennis Court Road, Cambridge, CB2 1QW, UK

[†] current address: Department of Microbiology, Faculty of Pharmacy, Meijo University

[€] current address: Evotec Ltd, 114 Park Dr, Innovation Dr, Abingdon, OX14 4RZ, UK

[¶] current address: Howard Hughes Medical Institute and Department of Biology, Brandeis University, Waltham, MA 02454, USA

[&] current address: Laboratory of Tissue Biology and Therapeutic Engineering, CNRS UMR 5305, University Claude Bernard-Lyon 1 and University of Lyon, 7 Passage du Vercors, 69367 Lyon Cedex 07, France

[±] current address: Triple Helical Peptides Ltd, Cambridge CB22 5DU

[§] corresponding authors, equal contribution senior authors

Acknowledgements

M3-specific antibodies were kindly provided by Professor Gunnar Lindahl, Lund University. We are grateful to Dr Susanne Talay for the M3-encoding pGEX6P-1 vector. The authors thank Dr Conny Yu for preparing a batch of M3-NTD for biofilm experiments. We thank the i04 and i24 beamline staff at the Diamond Light Source synchrotron for their help with data collection.

Funding

This research was funded by the Medical Research Council (MR/N009681/1), grants from European Union FP6 ASSIST (032390) and FP7 INFECT (305340), the Swedish Research Council (2022-01-202), and Region Stockholm, Center for Innovative Medicine (FoUI-975603).

Abstract

The M protein is an essential virulence factor of *Streptococcus pyogenes*, or group A streptococcus (GAS), one of the most common and dangerous human pathogens. Molecular and functional characterization of M protein variants and their interactions with host components is crucial for understanding streptococcal pathogenesis and vaccine development. The M3 protein is produced by the prevalent *emm*3 GAS serotype, which is frequently associated with severe invasive diseases. Here we characterize the interaction of M3 with human collagens through detailed structural and biochemical binding analysis. High-resolution structures of the N-terminal M3 domain in the free state as well as bound to a collagen peptide derived from the Collagen Ligands Collection reveal a novel T-shaped protein fold that presents binding sites complementing the characteristic topology of collagen triple helices. The structure of the M3/collagen peptide complex explains how *emm*3 GAS and related streptococci, such as the emerging human pathogen *Streptococcus dysgalactiae* subsp. *equisimilis*, can target collagens to enable colonization of various tissues. In line with this, we demonstrate that the M3/collagen interaction promotes enhanced biofilm formation of *emm*3 GAS in an *emm* type specific manner, which can be inhibited with the recombinant M3 N-terminal domain fragment. Further, *emm*3 GAS are shown to colocalize with collagen in tissue biopsies from patients with necrotizing soft tissue infections, where GAS biofilms are common. This observation is reproduced in infected organotypic skin models. Together, these data provide detailed molecular insights into an important streptococcal virulence mechanism with implications for the understanding of invasive infections, strategies for treating biofilm and M-protein based vaccine design.

Introduction

Streptococcus pyogenes (group A streptococcus, GAS) is one of the most prevalent human pathogens. It causes acute diseases ranging from trivial to life-threatening, such as pharyngotonsillitis (strep throat), scarlet fever, impetigo, meningitis, necrotizing fasciitis and streptococcal toxic shock-like syndrome [1]. The highest disease burden is caused by the post-infection sequelae acute rheumatic fever, rheumatic heart disease and glomerulonephritis [2, 3] but there is also a worrying global rise of severe invasive infections [4]. A key virulence factor involved in many if not all these diseases is the GAS M protein. Encoded by the chromosomal *emm* gene, the M protein is covalently anchored at its C-terminus to the cell wall, covering the GAS surface at high density and acting as an adhesin and a potent immune evasion factor [5-7]. M proteins are known, or can confidently be predicted, to form linear fibrils extending approximately 50 nm from the bacterial surface [8, 9]. Their hair-like architecture is based on dimerization of α-helical chains into parallel coiled coils, the defining and dominant structural feature of this class of proteins. Whilst sharing similar overall structure, M proteins are sequentially highly diverse, with over 220 distinct known variants of the *emm* gene defining GAS serotypes [10]. The C-terminal regions of M protein variants are highly conserved and predicted to form well-defined coiled coils. Sequences diverge increasingly towards the N-terminal hypervariable region (HVR) that is projected away from the bacterial surface. Experimental high-resolution structural information for M proteins is limited [11-14].

In addition to their role in adhesion and subverting the host's immune response, M proteins have also been implicated in biofilm formation [15]. Bacterial biofilms are a major cause of difficult-to-treat infections largely contributed by their recalcitrance to antibiotics and immune responses [16]. They are classified as either surface-attached biofilms, typically associated with implants and medical device-associated infections, or non-surface-associated biofilms. The latter are commonly observed in respiratory infections of patients with impaired mucociliary function, and in persistent soft tissue infections seen in chronic wounds resulting from diabetes or impaired vascularization [17]. Biofilm is also a potentially complicating feature associated with severe invasive GAS diseases. Analyses of biopsies collected during the acute phase identified biofilm in over 30% of patients with necrotizing soft tissue infections caused by GAS [18]. Some GAS types, such as *emm*1 and *emm*3, are over-represented among isolates from severe invasive infections, i.e. necrotizing soft tissue infections and streptococcal toxic shock syndrome [1, 19, 20], but no clear association between biofilm formation and *emm* type is known [21]. Köller *et al.* highlighted that the propensity of GAS to form biofilm *in vitro* was directly dictated by the experimental setting where both the medium and coating with specific extracellular matrix proteins influenced the outcome [22].

M proteins have been reported to interact with a wide range of host proteins, such as fibrinogen [23], C4-binding protein [24], plasminogen [25], fibronectin [26], collagens [27] and immunoglobulins [28].

108 Importantly, binding activities vary between *emm* types. Phylogenetic clusters of M proteins broadly
109 share binding propensities [10]. However, very few M protein interactions have been confirmed
110 through biophysical and structural analyses. The M1 protein binds to the fibrinogen D domain in the
111 variable "B-repeat" region [11]. Several M protein types have the ability to bind to the C4-binding
112 protein through their HVRs [14]. While these two molecular complexes rely on the dimeric coiled-coil
113 topology of the M proteins, the plasminogen kringle-2 domain binds to monomeric, non-coiled
114 segments of certain M proteins [29, 30].
115 In a screening of GAS strains belonging to 43 *emm* types, only *emm3* and *emm18* strains were
116 identified by Dinkla *et al.* to bind collagen IV to their surface [27]. For *emm3* isolates, this interaction
117 was demonstrated to depend on direct binding of collagen to the M3 protein. For *emm18* GAS
118 strains, binding was mediated by the hyaluronic acid capsule rather than the M18 protein. Direct
119 collagen binding has also been reported for M1 protein [31]. Based on available evidence, collagen
120 binding is not a universal property of GAS M proteins, but appears to be common among M proteins
121 of group C and G streptococci (*Streptococcus dysgalactiae* subsp. *equisimilis*, SDSE) [32, 33], which
122 are emerging as important human pathogens that share disease manifestations and virulence traits
123 with GAS [34, 35].
124 Collagens are commonly targeted by a wide range of pathogenic bacteria for the purposes of tissue
125 colonization and dissemination [36, 37]. They have been shown to interact directly with several
126 bacterial adhesins, such as CNA from *Staphylococcus aureus* [38], YadA from *Yersinia*
127 *enterocolitica* [39], and CNE from *Streptococcus equi* subsp. *equi* [40]. In the latter two cases,
128 adhesin binding has been mapped using the peptide libraries applied in the present study. While the
129 biological role of collagen binding by GAS is unknown, it has been linked to the induction of an
130 autoimmune response associated with post-streptococcal sequelae [27, 41]. The collagen IV binding
131 site in M3 was mapped to the N-terminal half of the protein [27]. Subsequently, a collagen-binding
132 sequence motif that is conserved in the HVRs of some M proteins of group A, C and G streptococci
133 was identified – the "peptide associated with rheumatic fever" (PARF) [33]. This motif is found in a
134 region predicted to deviate from the canonical coiled coil structure in M3, several other M proteins
135 and their homologs in non-group A streptococci (Figure 1). Binding of M3 protein to other collagen
136 types has not been reported, but the M protein FOG (aka Stg11) of SDSE was found to bind to
137 collagens I and IV [33, 42].
138 To gain insights into mechanism and biological role of streptococcal collagen binding, we
139 characterised the interaction of M3 with the Collagen Ligand Collections (CLCs, triple-helical
140 collagen peptide libraries formerly known as Toolkits), and determined crystal structures of the M3
141 N-terminal domain (M3-NTD), encompassing the HVR, alone and in complex with a CLC-derived
142 collagen peptide. We find that M3-NTD folds into a novel T-shaped domain that binds promiscuously
143 to collagen triple helices. Furthermore, we demonstrate that the M3-collagen interaction underpins

biofilm formation by GAS *emm3* isolates from necrotizing soft tissue infections, which can be inhibited *in vitro* by recombinant M3 protein.

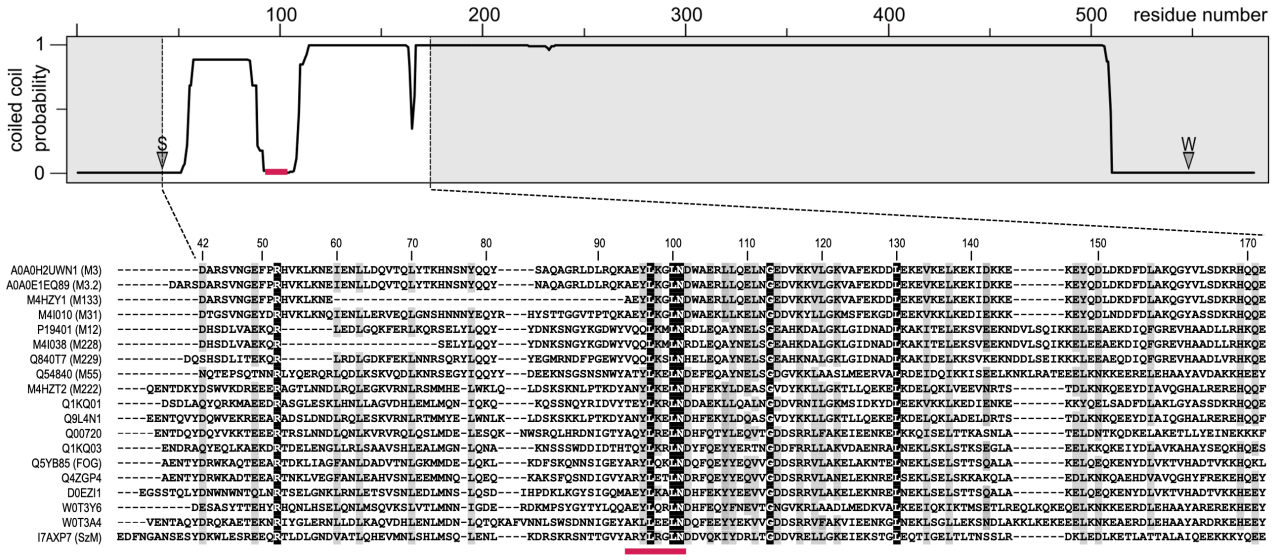

Figure 1. Multiple sequence alignment of the hypervariable regions of streptococcal M proteins. The top panel shows a MARCOIL coiled coil prediction [43] for full-length M3 protein. Positions of signal and wall anchor cleavage sites are indicated by S and W, respectively. The PARF motif (position indicated by pink bar), previously suggested to be required for collagen binding, resides in a region of M3 that is predicted to not adopt coiled coil topology. In the alignment, sequence similarity is indicated by grey shading for residues conserved or similar in at least 75% of sequences. 100% conserved residues are highlighted by black shading. Uniprot identifiers are shown to the left of the alignment. Sequences are ordered by alignment score. The proteins are from the following species: *Streptococcus pyogenes*: A0A0H2UWN1 (M3), A0A0E1EQ89 (M3.2), M4HZY1 (M133), M4I010 (M31), P19401 (M12), M4I038 (M228), Q840T7 (M229), Q54840 (M55), M4HZT2 (M222); *Streptococcus dysgalactiae* subsp. *equisimilis*: Q1KQ01, Q9L4N1, Q00720, Q1KQ03, Q5YB85, Q4ZGP4, D0EZI1, W0T3Y6, W0T3A4; *Streptococcus equi* subsp. *zooepidemicus*: I7AXP7.

Results

Recombinant M3 protein binds to the triple-helical domain of collagens II and III

The first aim of this study was to confirm the collagen binding activity of streptococcal M3 protein, and to identify any specific binding sites in collagen. To reduce the complexity of the experimental system we chose collagens II and III, as these are homotrimers, in contrast to, for instance, heterotrimeric collagens I and IV [44]. Recombinant M3 protein, lacking the N-terminal secretion signal and the C-terminal membrane-spanning region was produced in *Escherichia coli* as a glutathione S-transferase (GST) fusion protein. Binding to collagens II and III was investigated using

CLCs, libraries of 56 and 57 overlapping triple-helical peptides, respectively, covering the entire triple-helical tropocollagen domain of these two collagen types (1014 and 1029 amino acids) [45]. Recombinant M3 was found to bind to CLC peptides to various degrees, as quantified by an ELISA-like approach using an anti-GST antibody (Figure 2). While there were clear differences in binding between the CLC peptides, it was impossible to identify sequence features that were conserved in good binders (high apparent affinity) but absent from peptides that gave rise to signals comparable to negative controls. Neither sequence motifs, nor amino acid composition of the peptides (e.g., presence of hydroxyprolines, charged, hydrophobic or aromatic residues) were distinct in good binders. To investigate further the sequence requirements for M3 binding, we ranked the CLC peptides in decreasing apparent affinity, measured as A_{450} determined in the solid-phase binding assay, and then analyzed the distribution of particular amino acids in the entire set, pooling data from CLC-II and CLC-III. After background subtraction, we defined three binding groups: high affinity, having A_{450} between 0.5 and 0.75; medium affinity, A_{450} from 0.25 to 0.5; and low affinity, A_{450} from 0 to 0.25.

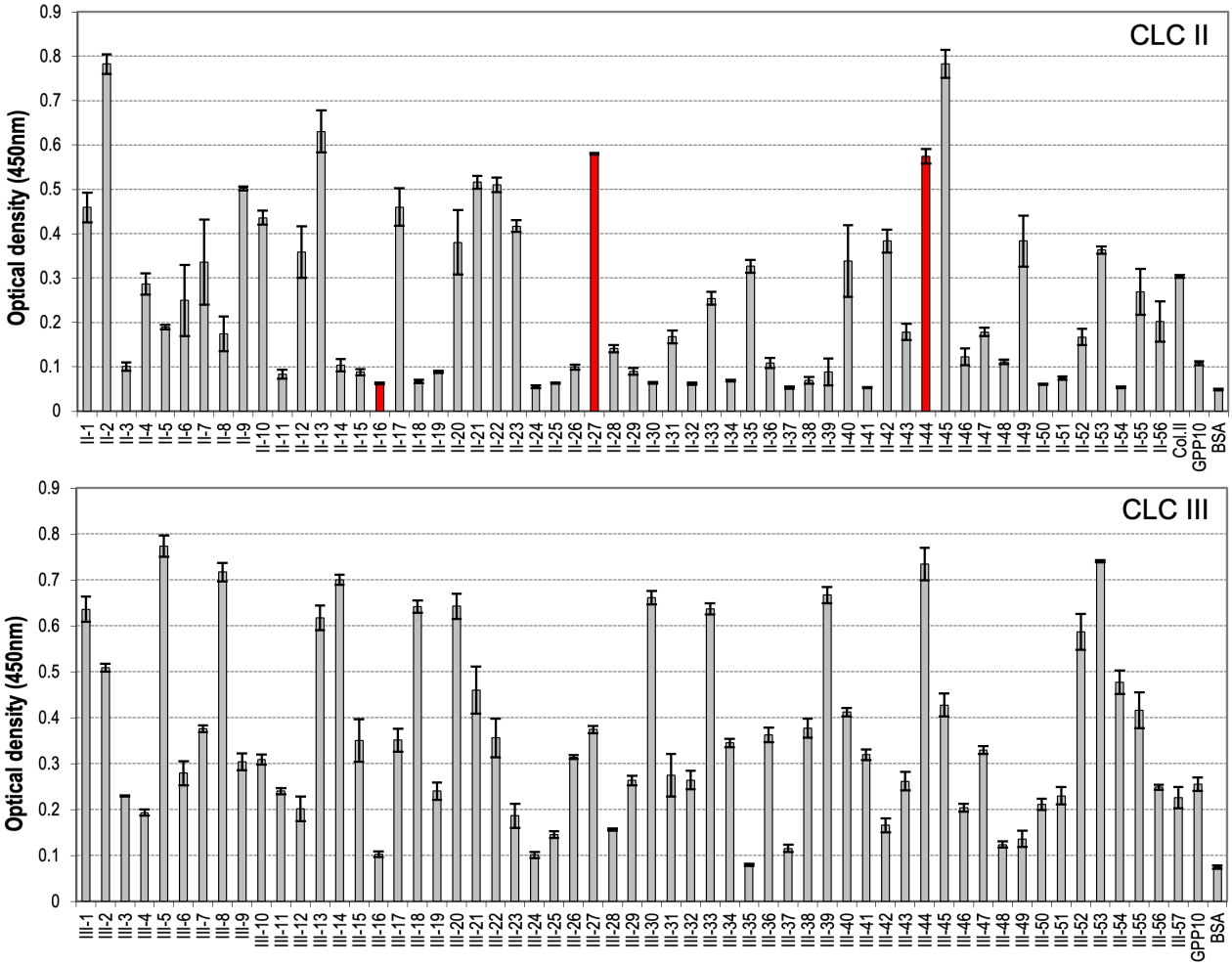

Figure 2. Binding of full-length M3 protein fused to GST to immobilised CLC II and III peptides. ELISA signal based on GST antibody is plotted against peptides spanning the tropocollagen (triple-helical)

188 regions of collagens II and III, as well as positive (collagen II) and negative (GPP10, BSA) controls.
189 Signals for three peptides chosen for further binding experiments are highlighted in red.

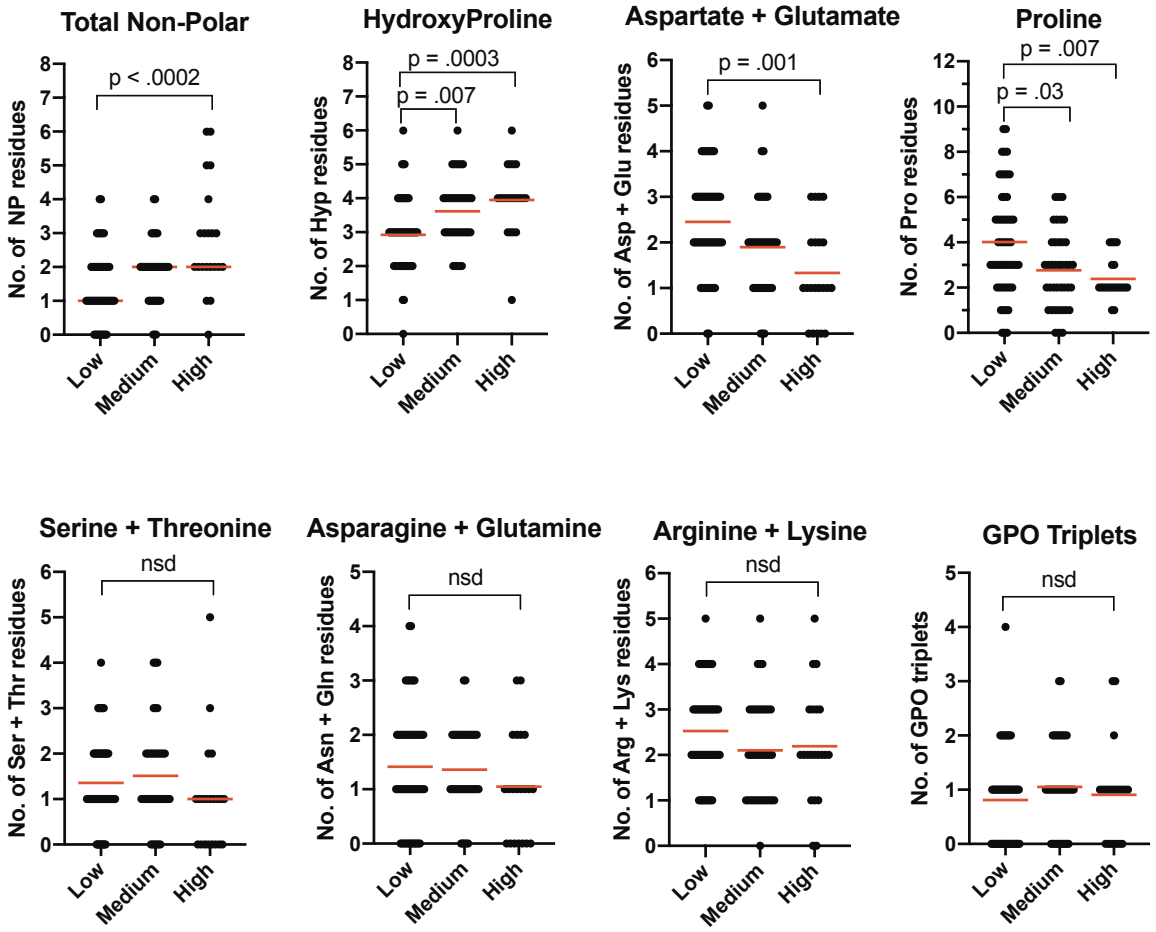

190
191 Figure 2—figure supplement 1: The Figure shows the number of specific residues or residue classes
192 per CLC peptide (y-axis) plotted versus rank group (x-axis). Groups are defined as low affinity (A450
193 = 0 to 0.25), medium affinity (A450 = 0.25 to 0.5) and high affinity (A450 = 0.5 to 0.5) in the solid
194 phase binding assays. Statistical difference between numbers in each group was determined by
195 non-parametric testing as defined in Methods.
196
197 We counted residues of each type in these three groups and compared their occurrence in peptides
198 of the three binding groups using non-parametric tests (Figure 2—figure supplement 1). The
199 outcomes are summarized in Table 1. Hydrophobic amino acids and hydroxyprolines appear to be
200 more frequent in good binders, while prolines and acidic residues are underrepresented. The
201 negative effect of proline on binding may explain why the $[GPP]_5$ flanking sequences of the CLC
202 peptides do not dominate binding to M3, allowing marked sequence selectivity to be observed in the
203 binding assays.
204
205

206 Table 1: Effect of amino acid classes on binding of M3 to CLCs.

Amino Acid class	Effect on binding rank	Significance
Hydrophobic (F, L, V, M, I)	Positive	p = .0002
Hydroxyproline (O)	Positive	p = .0003
Polar (S, T)	None	
Polar (Q, N)	None	
Basic (R, K)	None	
GPO triplets	None	
Acidic (D, E)	Negative	p = .001
Proline (P)	Negative	p = .0007

207

208 ***M3-NTD harbors the collagen binding site***

209 Full-length M proteins are not amenable to high-resolution structural characterization due to their
210 anisotropic shape and potential conformational dynamics. We therefore designed a construct
211 representing the M3 N-terminal domain (M3-NTD), which comprises the HVR and a short region
212 predicted to adopt a dimeric coiled-coil structure. This fragment would not only allow structural
213 characterization but could also be used to confirm the previously suggested localization of the
214 collagen binding site at the HVR [33]. M3-NTD includes the 110 N-terminal residues of mature M3
215 (residues 42-151 of the M3 protein precursor sequence). To stabilize a dimeric conformation, Leu151
216 was replaced with a cysteine for disulfide bond formation at the C-terminus. Leu151 is predicted to
217 occupy a "d" position in the canonical coiled coil heptad pattern, forming part of the hydrophobic
218 interface between the α-helices, a position ideally suited for disulfide bond formation [46]. A ^{15}N
219 isotopically labelled version of M3-NTD was made for NMR spectroscopic analysis. From a
220 comparison of ^{1}H, ^{15}N heteronuclear single-quantum coherence (HSQC) spectra it is evident that a
221 significant structural change occurred upon oxidation (resulting in disulfide bond formation) of the
222 protein. The higher dispersion of signals, most noticeably in the ^{1}H dimension, indicates disulfide-
223 linked M3-NTD adopts a folded conformation (Figure 3A). In contrast, the reduced, monomeric form
224 gives rise to a poorly resolved spectrum with signals falling within the random-coil chemical shift
225 range, and big differences in crosspeak intensities that suggest dynamic behavior (Figure 3B). This
226 demonstrates the C-terminal disulfide bond is required to stabilize a dimeric, folded structure that
227 differs from extended unfolded or linear α-helical conformations.

228 To test if M3-NTD harbors the collagen binding site, binding to selected CLC triple-helical peptides
229 was studied by isothermal titration calorimetry (ITC). We selected two peptides that showed medium
230 to high apparent affinity in the CLC screening (II-27 and II-44) and a low affinity peptide (II-16). These
231 three peptides all interacted with M3-NTD in solution (Figure 4A-C). II-27 and II-44 binding was
232 characterized by dissociation constants (K_D) in the low micromolar range (7 and 5 μM, respectively).
233 II-16 had an approximately ten times lower affinity (K_D = 70 μM) for M3-NTD. These K_Ds reflect the

differences in binding of full-length M3 evident from the CLC solid-phase binding assay. Fitting of the sigmoidal binding curves for II-27 and II-44 suggested two indistinguishable collagen binding sites per M3 dimer. To assess if the interaction was dependent on the triple-helical conformation of the CLC peptides, we titrated M3-NTD into a monomeric version of II-44 with scrambled GPP repeat sequences at the termini [47]. No binding was observed (Figure 4D). To test if collagen peptide binding required the M3-NTD to adopt its dimeric fold, the reduced (monomeric) form of M3-NTD was titrated into trimeric II-44 (Fig. 4E). The titration curve reflected weak binding, with data not suitable for fitting. Weak binding is in line with the observation that peptides representing the PARF motif in collagen-binding M proteins have some ability to bind to collagen IV in a spot-membrane assay [33].

In conclusion, the collagen binding site of M3 was confirmed to reside in M3-NTD. CLC solid-phase binding results obtained for full-length M3 align with in-solution interaction analyses by ITC using M3-NTD. Binding of M3-NTD to collagen peptides depends on their triple-helical structure, and on the dimeric conformation of M3-NTD.

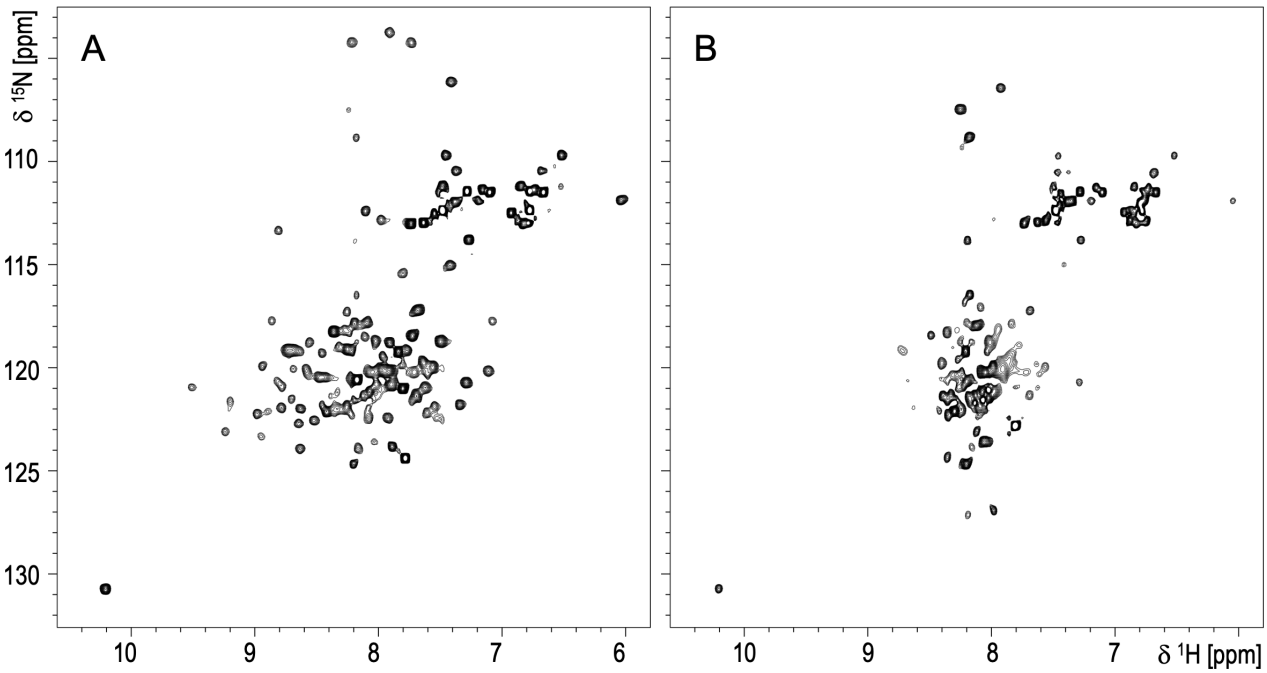

Figure 3. $^{1}H,^{15}N$ HSQC spectra for (A) disulfide-bond stabilized dimeric M3-NTD and (B) the reduced, monomeric form.

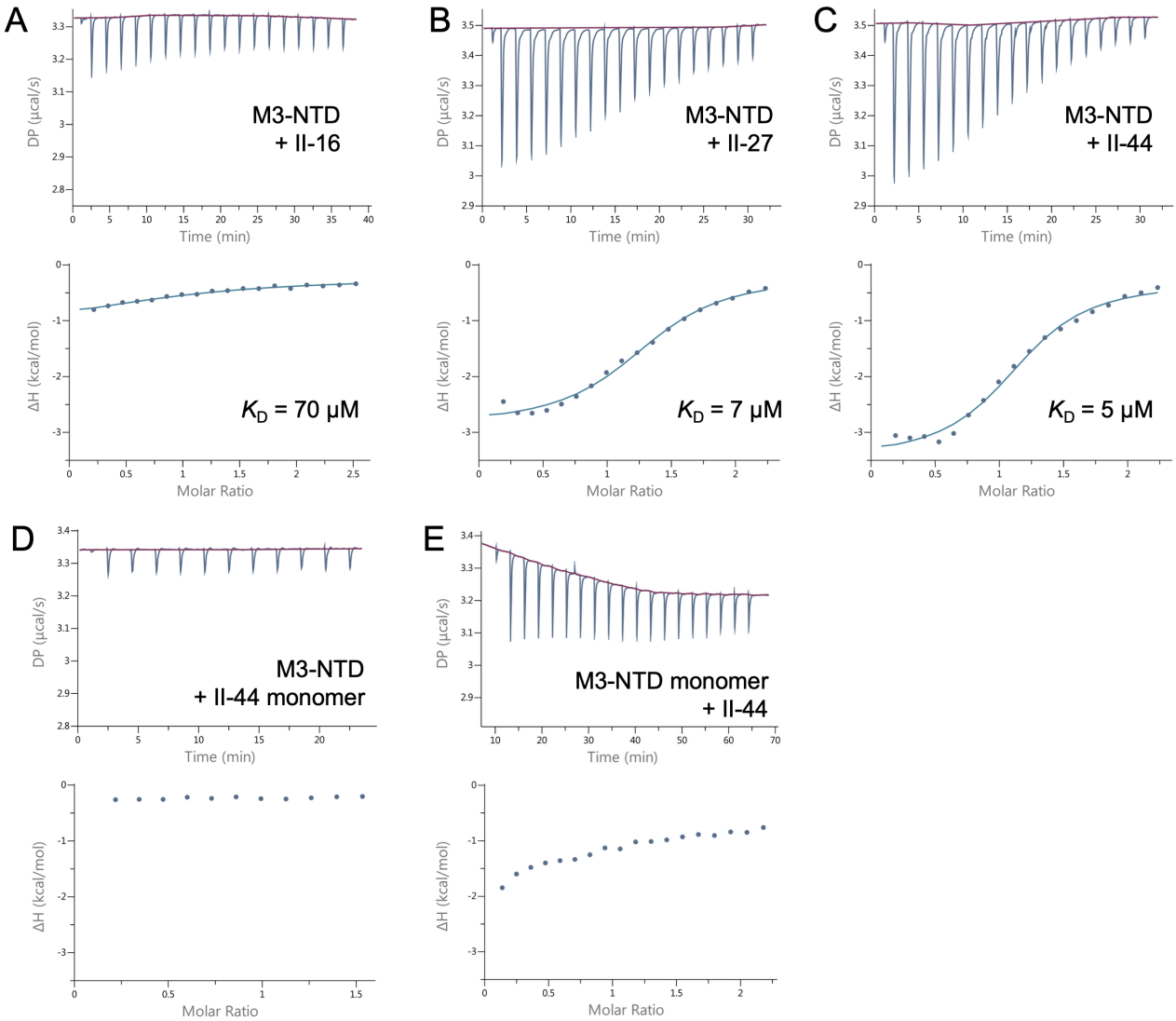

Figure 4. ITC binding curves for M3-NTD interactions with CLC peptides. Top panels show heat responses to repeated injections of M3-NTD into collagen peptide solutions, with baselines shown in red. Bottom panels shown integrated signals (enthalpy changes) plotted against the molar ratio of binding partners. Where non-linear fitting gave meaningful results, the fits are shown as blue lines, and dissociation constants (K_D) are specified.

M3-NTD adopts a folded structure deviating from dimeric coiled coil

M3-NTD crystallized in several conditions with the best crystals diffracting X-rays to a resolution of 1.9 Å at the synchrotron radiation source. Phasing and structure determination was achieved using a selenium single-wavelength anomalous diffraction (Se-SAD) dataset at 2.6 Å resolution with the final model refined against the native data set at 1.9 Å resolution (Table 2).

M3-NTD is a symmetrical homodimer, linked at the C-terminus by a disulfide bond (Figure 5A). The first three residues of the construct (Gly-Ala-Met), a cloning artefact, are not resolved in the structure.

268 Table 2: Data collection and refinement statistics. Values in brackets refer to the highest resolution
269 shell.

	M3-NTD	**SeMet M3-NTD**	**M3-NTD+JDM238**
Data collection	**8P6K**		**8P6J**
Spacegroup	C2	C2	P1
Cell dimensions			
a, b, c (Å)	150.5, 24.1, 78.0	150.4, 25.1, 77.0	31.8, 51.5, 80.2
a, b, c (°)	90, 105.3, 90	90, 104.4, 90	87.3, 84.8, 89.4
Resolution (Å)	37.62 - 1.92 (1.94 - 1.92)	37.3 – 2.67 (2.71 – 2.67)	79.77 - 2.32 (2.45 - 2.32)
R_{meas}	0.058	0.198	0.107
I/σ	14.8	10.2	2.1
$CC_{1/2}$	0.9 (0.5)	1 (0.9)	1 (0.3)
Completeness (%)	97.80 (94.07)	98.8	89.58 (89.66)
Multiplicity	6.2	18.6	1.7
Refinement statistics			
Resolution (Å)	37.6 - 1.92		79.77 - 2.32
No. reflections	21411 (1054)		19530 (947)
R_{work}/R_{free}	0.230/0.268		0.241/0.285
Ramachandran favoured (%)	97.7		97.7
Ramachandran outliers (%)	0		0.5
RMS deviations			
Bond lengths (Å)	0.039		0.013
Bond angles (°)	2.06		1.89

270

271 The fold represents a novel T-shaped architecture with no significantly similar structures identifiable
272 by the protein structure comparison server DALI [48]. Each monomer is composed of three α-helices,
273 H1-H3. The H3 helices comprise the C-terminal 38 residues of M3-NTD (M3 residues 114-151) and
274 form a coiled coil stem. This, in the full-length protein, would be extended into a ~50 nm long coiled
275 coil characteristic of M proteins (Figure 5B). Helices H1 and H2 form hairpins that pack against each
276 other to form the slightly kinked bar of the T-shape, effectively a three-helix bundle. A key residue is
277 Gly113, which resides at the T-junction, separating H2 and H3 (Figure 5C). It is completely
278 conserved in M proteins identified in our sequence similarity search (Figure 1). The T-junction
279 structure is defined by conserved leucine and isoleucine residues that form a small hydrophobic core
280 (Figure 5C). The T-bar structure is stabilized by a network of polar interactions of several conserved
281 residues, most notably inter-chain salt bridges of Arg52 with Asp102 and Glu105, and an inter-chain
282 hydrogen bond between the side chains of Glu49 and Asn101 (Figure 5D). Asn101 is one of the
283 completely conserved residues in the PARF motif, previously implicated in collagen binding. This
284 motif is located on H2 at the bottom of the T-bar (Figure 5A). Some but not all conserved PARF
285 residues contribute to the formation of the T-bar structure of M3-NTD. Leu97 and Asn101 are the
286 only completely conserved residue of PARF with a structural role. Leu97 is buried at the interface

287 between the H1-H2 hairpin of one monomer and H1 of the other monomer, packing against the
288 Tyr81 sidechain (Figure 5D).

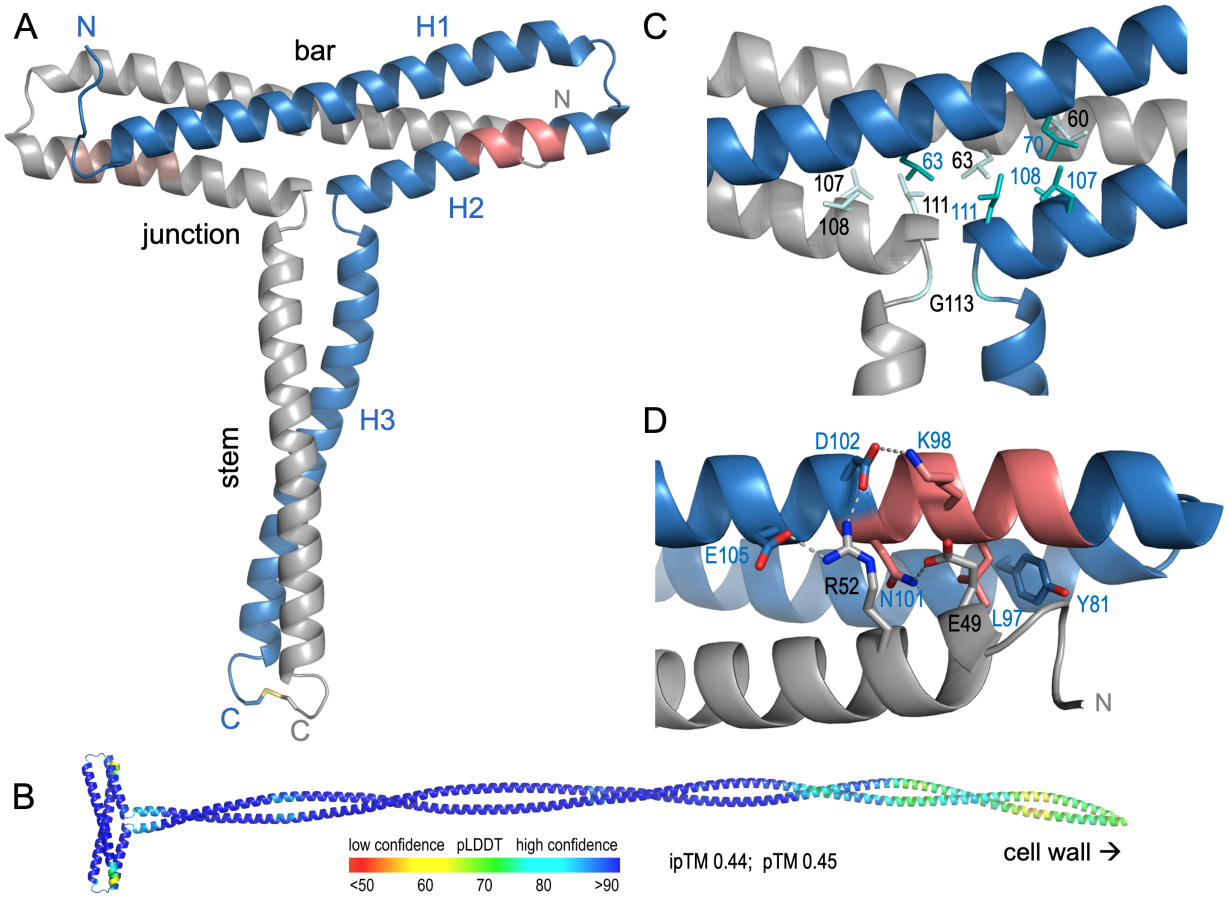

289

290 Figure 5. Crystal structure of M3-NTD (PDB 8p6k). A) Ribbon diagram of the covalently stabilized
291 M3-NTD dimer. Monomers are shown in blue and grey. The regions previously associated with
292 collagen binding (PARF motif) are highlighted in red. N-termini (Asp42) and C-termini (Cys151) are
293 labelled N and C, respectively. The three helices of the blue monomer are labelled H1-3. The C-
294 terminal disulfide bond is shown as sticks. B) Ribbon diagram model for the full extracellular region
295 of M3, predicted by AlphaFold3 [49] and colored by per-residue confidence (pLDDT). C) Conserved
296 leucine, isoleucine (Ile60) and glycine (Gly103) residues define the T-junction structure of M3-NTD.
297 D) Role of conserved residues around the PARF motif in stabilizing the T-bar region of M3-NTD.
298 Polar contacts are shown as dashed lines.

299

300 ***An N-terminal T-shaped fold is predicted to be a feature of other M proteins***

301 AlphaFold3 [49] predictions were carried out for the proteins identified in our sequence similarity
302 search (Figure 1) to support the structural role of the conserved residues. In validation of this
303 approach, the AlphaFold3 predicted model of M3 is almost perfectly superimposable with the
304 experimental M3-NTD structure (Figure 6A). All other proteins included in this study are predicted to
305 have T-shaped N-terminal domains, with exception of proteins M133 and M228, where deletions

306 break the topology of the T-bar fold (Figure 6B, Figure 6—figure supplement 1). Some of the
307 predictions for GAS M protein variants (M12, M55, M229) carry low confidence and these proteins
308 may well not adopt the T-fold. HVRs of M proteins that are phylogenetically more distant to M3, such
309 as M1 and M28, are not predicted to fold into any distinct tertiary structure deviating from coiled coil
310 (Figure 6C). On the other hand, M proteins of SDSE and the SzM protein of *Streptococcus equi*
311 subsp. *zooepidemicus* (SESZ) are predicted with high confidence to adopt a structure similar to M3.
312 This analysis structurally validates our sequence alignment of M3 homologs. It suggests the T-
313 shaped structure of the NTD is a feature of a subclass of M proteins and is common in SDSE.
314

315 ***M3-NTD binds promiscuously to the collagen triple helix***

316 M3-NTD is a structurally tractable fragment that retains the collagen binding activity of the full-length
317 protein. We chose II-27, a CLC peptide with good affinity for M3-NTD, as the basis for structural
318 characterization of an M3-collagen complex. II-27 contains an atypical $\alpha 1\beta 1$ integrin-selective motif,
319 GVOGEA [50]. To increase chances of crystallization, a shorter 24-residue peptide, JDM238, was
320 synthesized which contains the GVOGEA motif flanked by three glycine-proline-4-hydroxyproline

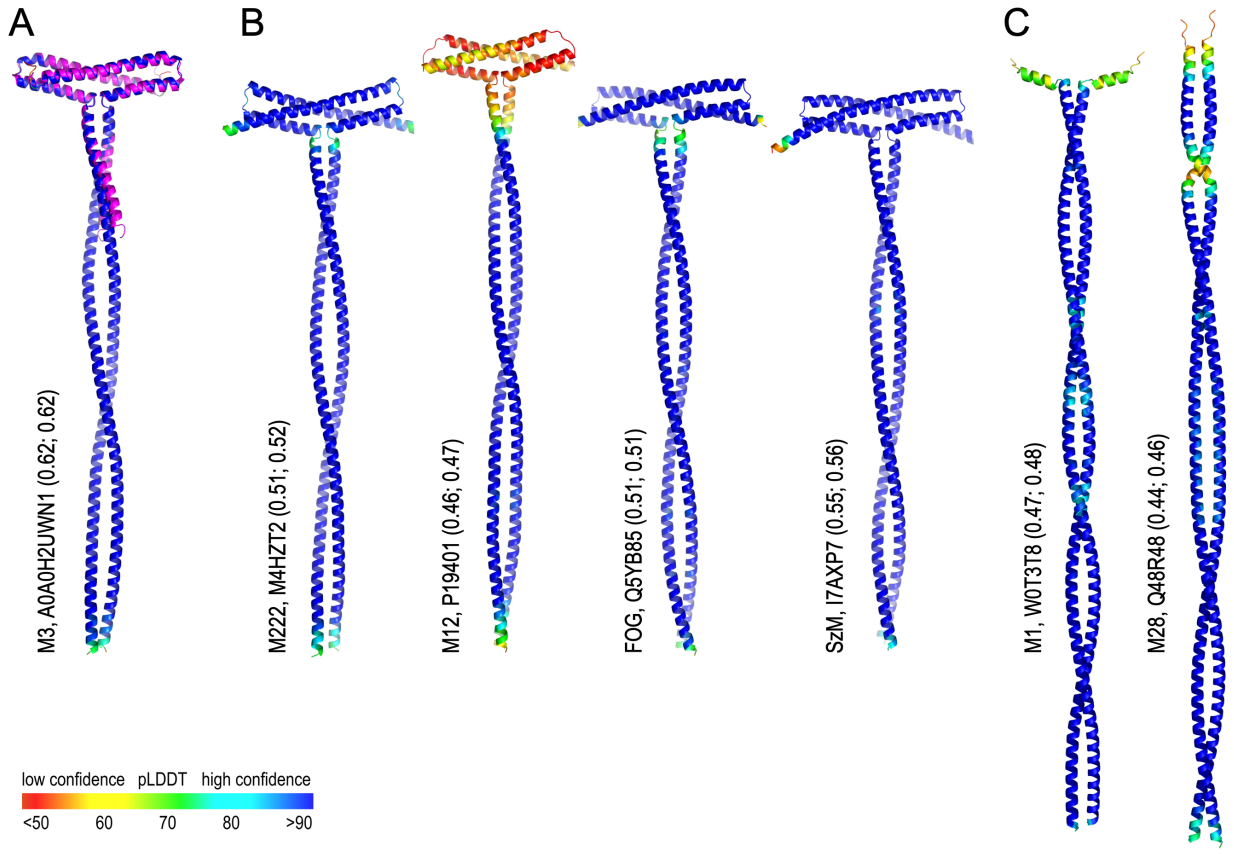

321

322 Figure 6. AlphaFold3 predictions for M proteins of GAS, SDSE and SESZ. A) Overlay of the
323 experimental M3-NTD structure (magenta) with a predicted structure for the N-terminal 230 residues
324 of mature M3 (coloured by pLDDT). B) Predicted structures for the N-terminal 230 residues of other
325 M proteins included in the sequence alignment (Figure 1). C) Predicted structures for the N-terminal

230 residues of M1 and M28 proteins, which are not known to interact with collagens. Values in parentheses are AlphaFold3 prediction quality parameters ipTM and pTM, respectively.

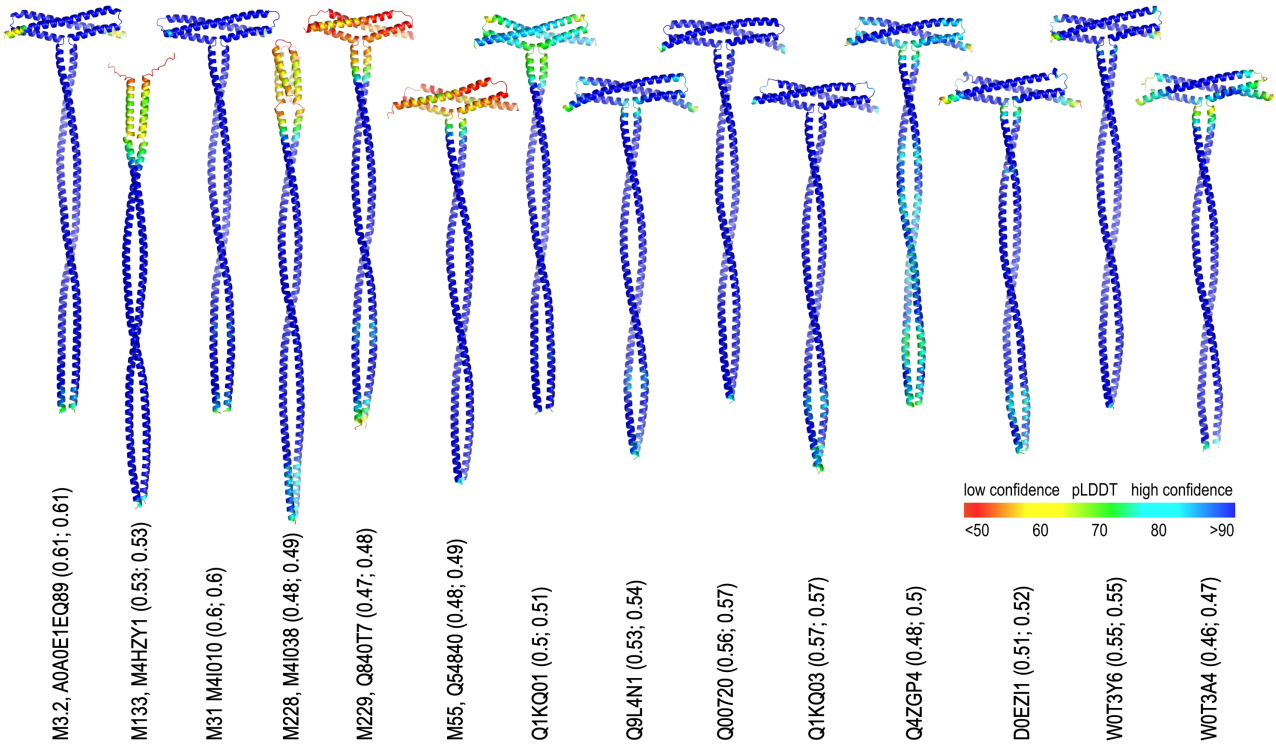

Figure 6—figure supplement 1. Additional AlphaFold3 predicted structures of proteins included in the sequence alignment (Figure 1). The N-terminal 230 residues of mature proteins were included in predictions (colored by pLDDT). For M133 only the first 196 residues have been modelled to highlight of the effect of the deletion of residues that are integral to the T-shape structure of M3. Values in parentheses are AlphaFold3 prediction quality parameters ipTM and pTM, respectively.

(GPO) repeats at each terminus. Crystals formed in conditions containing JDM238 and M3-NTD at a 3:2 molar ratio and diffracted synchrotron X-rays to 2.3 Å resolution. Molecular replacement with M3-NTD yielded a high-quality structural model for the complex (Table 2).

In agreement with our ITC data for CLC II-27 binding to M3-NTD, the M3-NTD dimer is bound to two copies of triple-helical JDM238. While both copies occupy equivalent binding sites on opposite faces of the M3-NTD T-bar, they contact the protein with two different regions (Figure 7). One copy contacts M3-NTD through residues 15-21 of the C-terminal GPO repeats, the other is bound at its more central GPOGVO region (residues 6-12) (Figures 7 and 8A). The presence of two different binding registers in the same crystal is likely an effect of crystal packing, as this binding mode results in a compact assembly required for crystallization (Figure 7—figure supplement 1), but it also reflects a lack of specificity of collagen binding by M3, in line with the CLC screening data. Superposition of

347 the two binding sites highlights how the M3-NTD T-bar complements the characteristic and uniform
348 surface topology of triple helices in both binding registers in the same fashion (Figure 8B).
349

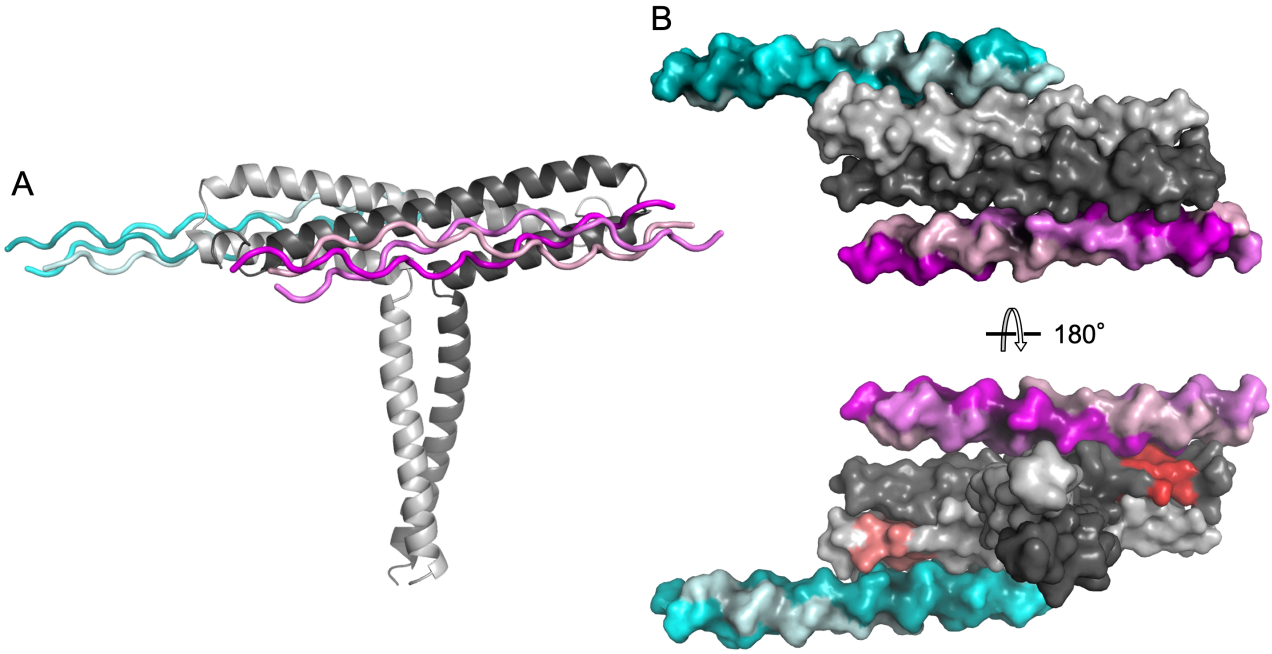

350
351
352 Figure 7. Structural basis of collagen binding by M3 (PDB 8p6j). A) Crystal structure of the complex
353 of M3-NTD (subunits shown in light and dark grey cartoon representation) with collagen-derived
354 peptide JDM238. Two binding registers are observed bound to equivalent sites of the M3-NTD dimer,
355 indicated by shades of magenta and cyan. B) Space-filling models of views from the top of the T-bar
356 of M3-NTD (top) and looking down the stem towards the bottom of the T-bar (bottom). The PARF
357 motif is shown in tones of red, otherwise coloring is as in A.
358

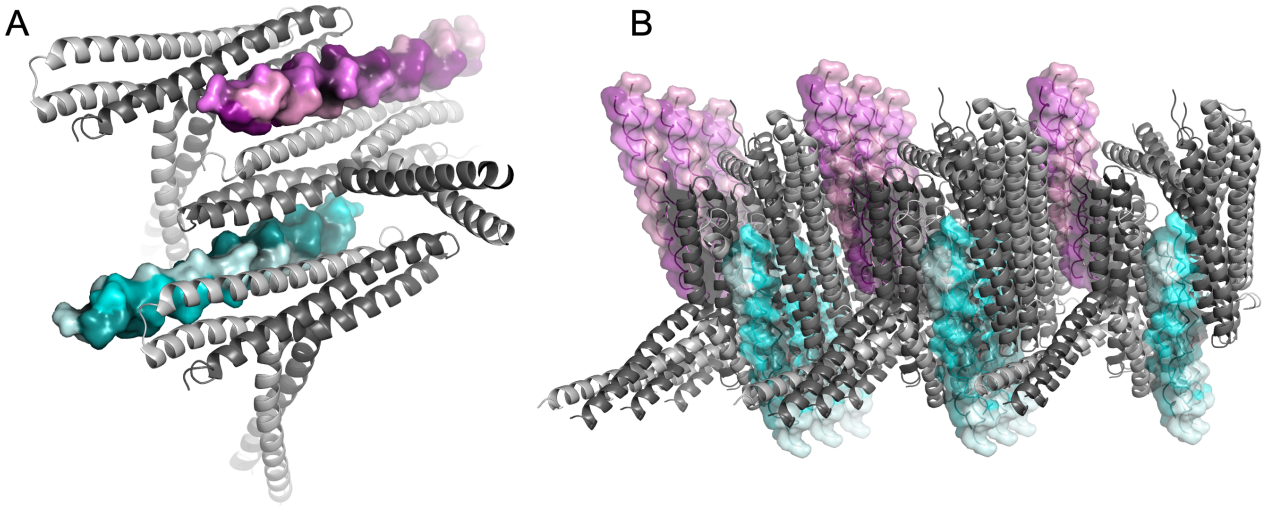

359

Figure 7—figure supplement 1: Crystal packing. (A) Each triple-helical peptide (shades of magenta and cyan) is bound to two copies of M3-NTD (grey ribbons) at two distinct sites. (B) This results in the compact assembly observed in the crystal.

The M3 collagen binding site includes the PARF region on H2 (residues 94-101), extending beyond it to include the C-terminal half of H1 and most of H2 (Figure 8). This confirms previous reports on the involvement of PARF in collagen binding [32, 33]. Interfaces between the binding partners largely comprise hydrophobic interactions between highly complementary surfaces. M3 residues Tyr96 and Trp103 play prominent roles: they pack against Hyp and Pro sidechains, filling grooves on the collagen triple helices and form polar contacts with the peptide backbone. The indole amino group of Trp103 interacts with the carbonyl of Ala15 or Hyp6 (depending on the register), while Tyr96 forms a water-mediated hydrogen bond with the carbonyl of Hyp9 or Hyp18. In one binding mode, M3 Gln42 hydrogen bonds with the same water molecule as Tyr96. Direct polar contacts also include M3 residues Lys35 and Arg49 which interact with the hydroxyl group of Hyp9 and the backbone carbonyl of Hyp12, respectively. In addition, in one binding mode M3 residue Gln46 forms a hydrogen bond with Gly22 of the peptide via a water molecule.

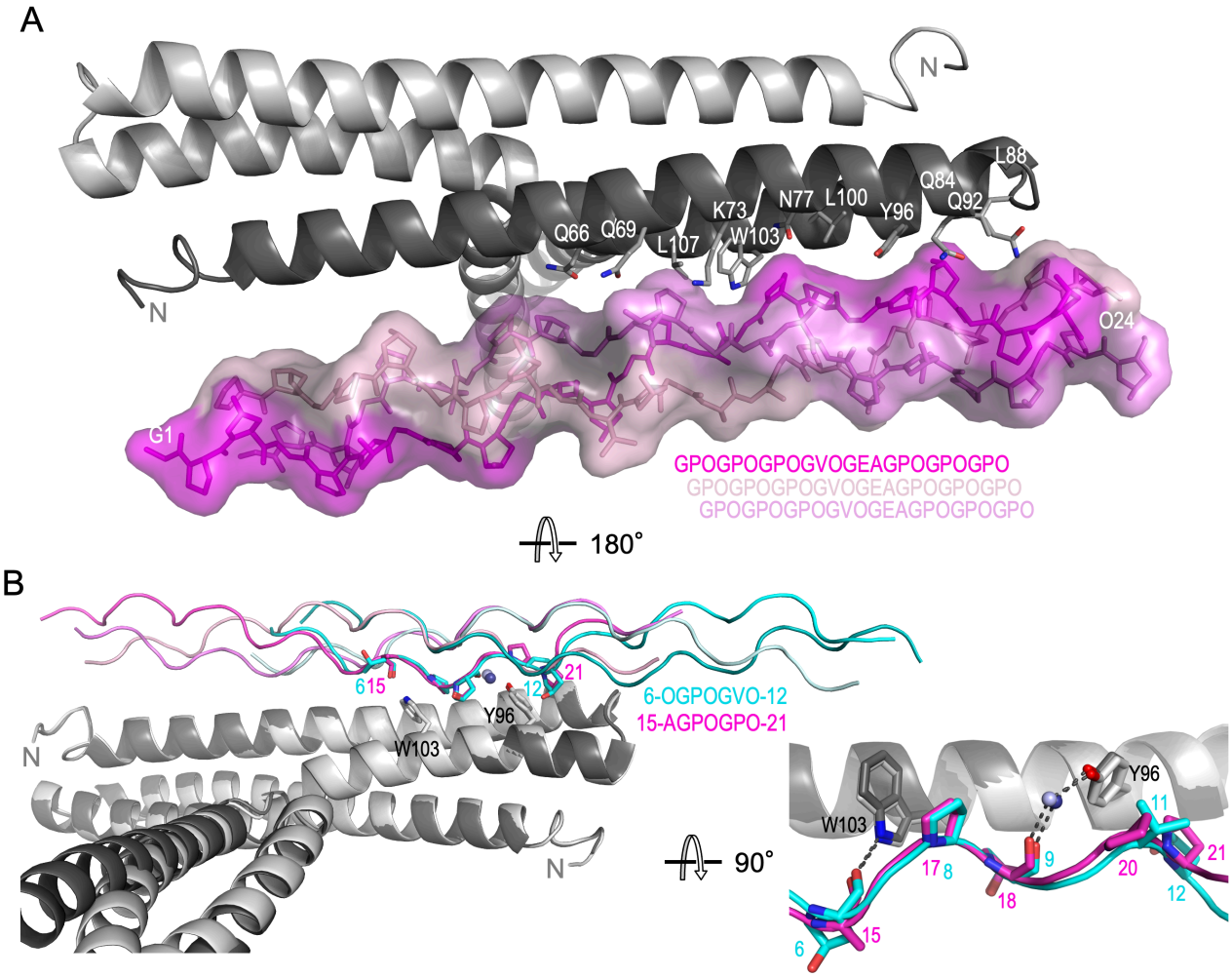

Figure 8. Collagen triple helix/M3-NTD interface. A) Residues of M3-NTD (grey cartoon representation) that form the collagen binding site are shown as sticks and are labelled. The collagen peptide triple helix is shown in stick and surface representation in shades of magenta. The sequence is shown indicating the staggered arrangement of the chains in the triple helix. B) Superposition of the two peptide binding sites to highlight conservation of collagen binding mode despite sequence deviation between the two binding registers. Tyr96 and Trp103 are shown as sticks. The two monomers of M3-NTD are shown in light and dark shades of grey. Collagen peptides of the two binding modes are shown in magenta and cyan, with five equivalent sidechains shown as sticks. The equivalent sequences of the binding sites are shown. Water molecules in the binding interface are shown as blue spheres. In the zoomed-in image on the bottom right, only one of the collagen peptide chains is shown per complex for clarity. Hydrogen bonds are shown as grey dashed lines.

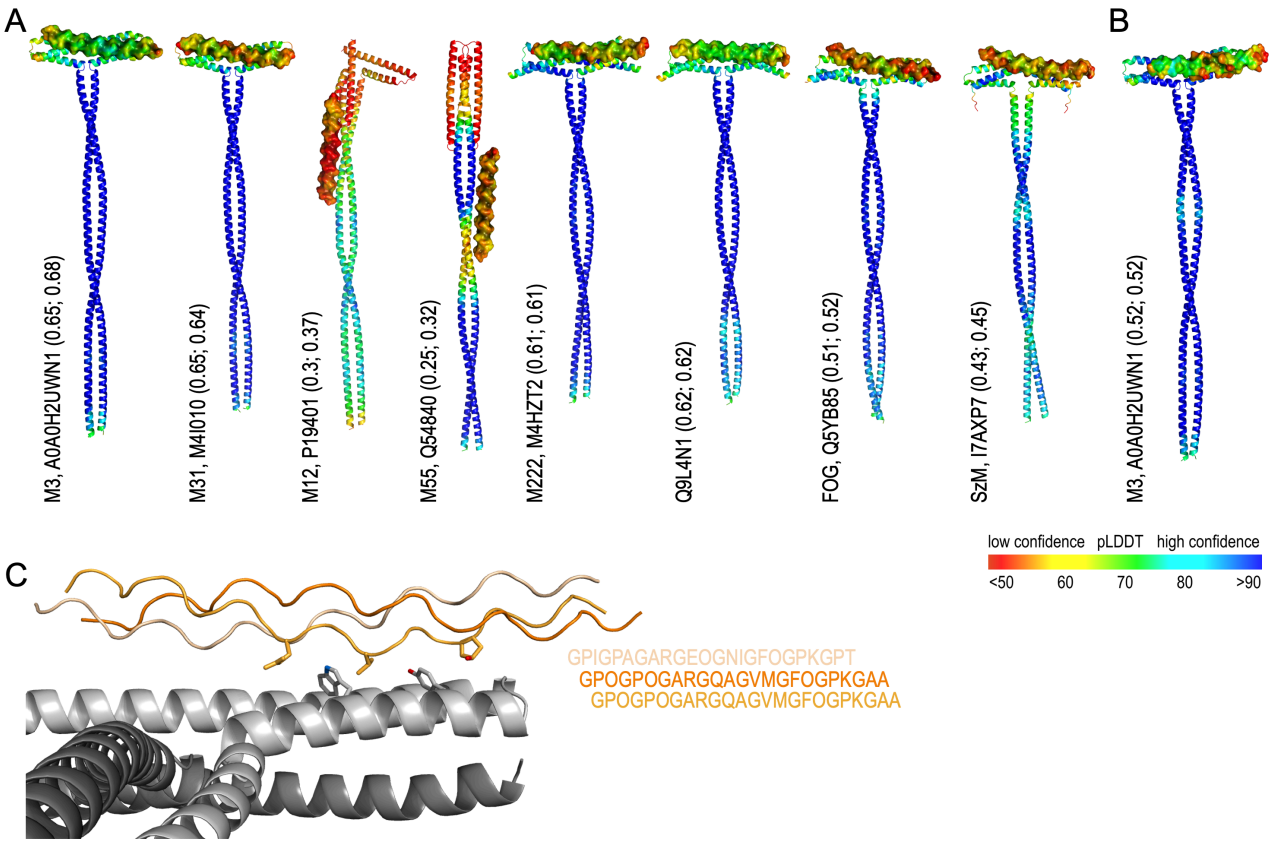

Figure 8—figure supplement 1: AlphaFold3 predicted structures of M proteins in complex with 24-residue collagen peptides. (A) Predicted complexes with the model collagen peptide (GPO_8), representing the generic tropocollagen triple-helical structure. Two chains of the N-terminal 230 residues of mature proteins and, for clarity, only three collagen peptide chains were included in predictions. M proteins are shown in cartoon, GPO_8 peptide in surface representations, respectively (coloured by pLDDT). Values in parentheses are AlphaFold3 prediction quality parameters ipTM and pTM, respectively. (B) Predicted structure of an equivalent complex between M3 and a type I

collagen peptide. (C) Closeup view of the predicted binding site of the type I collagen peptide (shades of orange) and M3 (shades of grey). Key residues, equivalent to the ones shown in Figure 8B, are shown in stick representation. The sequences of the hetero-triple-helical peptide (two α1 chains and one α2 chain), derived from PDB 5CTD, are also shown.

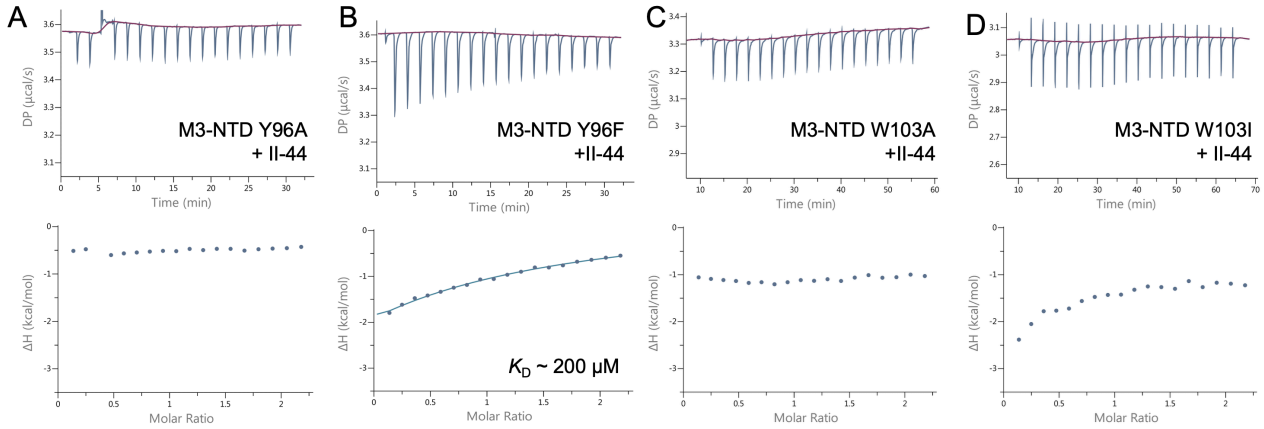

Figure 8—figure supplement 2. ITC binding curves for M3-NTD variants with peptide II-44. Top panels show heat responses to repeated injections of M3-NTD into II-44 solutions, with baselines shown in red. Bottom panels shown integrated signals (enthalpy changes) plotted against the molar ratio of binding partners. For M3-NTD Y96F the fit is shown as a blue line, and dissociation constant (K_D) specified.

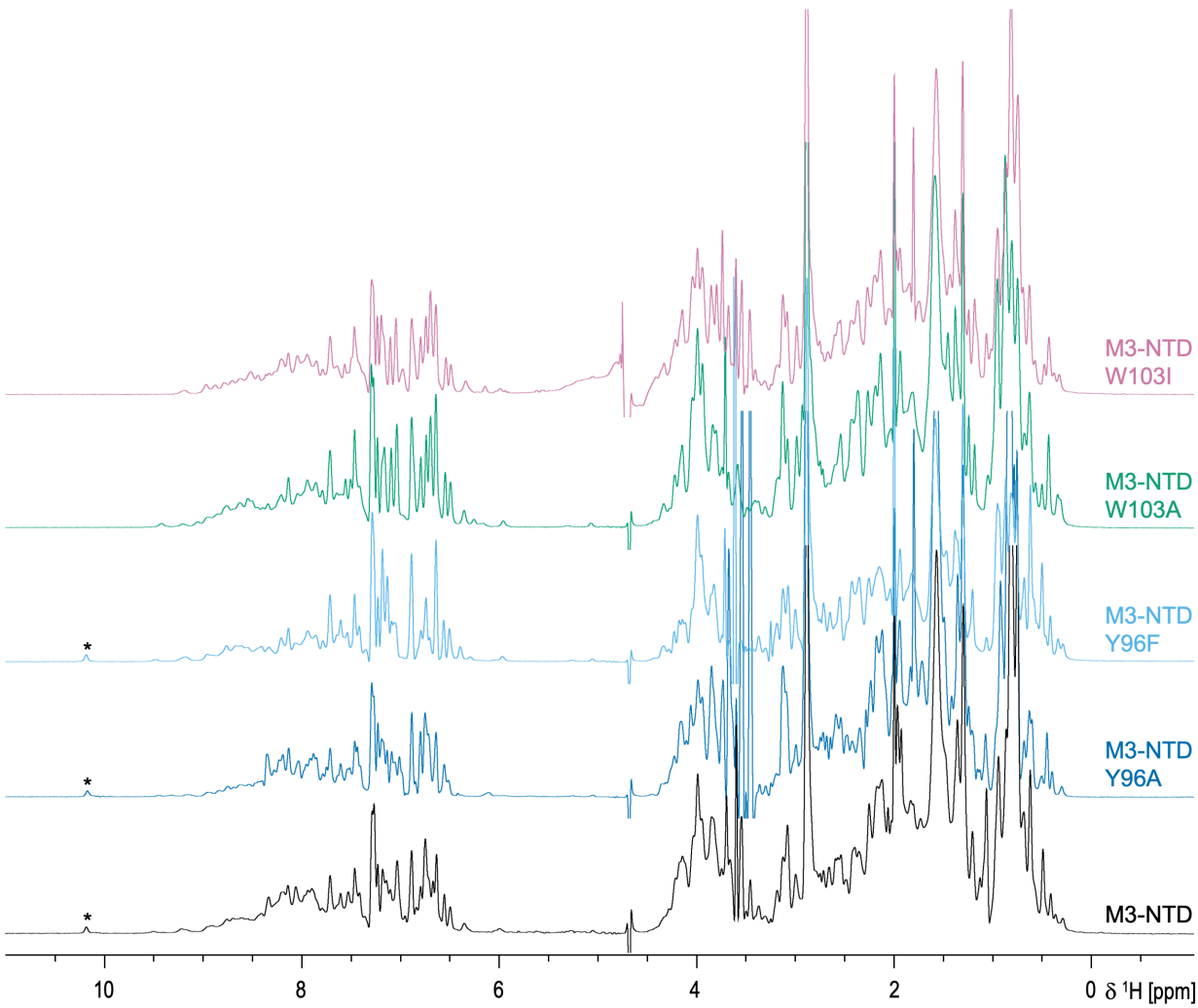

Figure 8—figure supplement 3. ^{1}H NMR spectra of M3-NTD and variants with key collagen-binding residues mutated. Asterisks, Trp103 indole NH signals.

Two M3 residues are required for collagen peptide binding

Tyr96 is a conserved residue of the PARF motif. We tested its role in collagen binding using two site-specific variants, Tyr96Ala and Tyr96Phe. When titrating M3-NTD Tyr96Ala into CLC peptide II-44, which bound to wild type M3-NTD with low micromolar K_D, no binding was observed (Figure 8—figure supplement 2). The more conservative substitution of Tyr96 with Phe also greatly reduced the affinity for II-44 (K_D ~200 μM) (Figure 4F), suggesting that the water-mediated interaction between Tyr96 and the peptide backbone strongly contributes to binding.

Similar results were obtained for Trp103, the second prominent residue in the M3/collagen interface. Mutation to an Ala led to a loss of binding as detected by ITC. Replacement of Trp by the large hydrophobic Ile resulted in detectable but weak binding, with data not suitable for non-linear fitting to derive meaningful thermodynamic parameters.

426 To rule out any effect of mutations of Tyr96 and Trp103 on the structure of M3-NTD, ^{1}H NMR spectra
427 were recorded (Figure 8—figure supplement 3). The spectra all showed very similar dispersion of
428 resonances, reflecting a folded state with some hydrophobic core giving rise to resonances below
429 0.5 ppm. The only readily assignable resonance, due to its unique chemical shift, is the indole NH
430 of Trp103, which, as expected, is lacking in the Trp mutants, but found at almost exactly the same
431 chemical shift in M3-NTD and the Tyr96 mutants. These data support the loss of affinity of collagen
432 peptides for the Tyr96 and Trp103 mutants being attributed to contribution of these residues to the
433 binding interface rather than a loss of structure, as would be expected from the crystal structures.
434 This supports the critical role of Tyr96 and Trp103 in collagen binding, both via forming van der
435 Waals interactions with the collagen peptide triple helix as well as forming direct and water-mediated
436 polar interactions with the peptide backbone.
437 In conclusion, we present the first structural evidence for an M-protein collagen complex. The
438 structure indicates a general binding mechanism that might explain the promiscuity of M3 for diverse
439 CLC peptides and explains how M3 is able to bind non-selectively to different collagen types, which
440 all share very similar triple-helical (COL) domains. This is supported by an AlphaFold3 prediction of
441 a complex between M3 and a type I collagen peptide, which is predicted to bind to M3 in a way that
442 is highly similar to the experimental complex structure (Figure 8—figure supplement 1B,C).
443
444 **emm *type-dependent effect of human collagen on biofilm formation by GAS strains***
445 GAS *emm*3 strains are highly prevalent in necrotizing soft tissue infections [19, 20], where they have
446 been found to form biofilm [18]. Based on our previous data demonstrating that the tissue milieu
447 seems to promote GAS biofilm [18], and with collagen being a ubiquitous structural protein, it was of
448 interest to assess whether the M3-collagen interaction could affect biofilm formation. For this
449 purpose, we used crystal-violet based assay to determine biofilm formation by GAS strains from
450 patients with necrotizing soft tissue infections on polystyrene plates, either uncoated or coated with
451 human type I collagen. The three isolates, *emm*1, e*mm*3 and *emm*28 strains, all formed biofilm on
452 uncoated plates (Figure 9A). Notably, on collagen-coated plates, biofilm of isolates 2006 (*emm*1)
453 and 5004 (*emm*28) was significantly reduced in a dose-dependent manner, while that of isolate 2028
454 (*emm*3) was significantly enhanced (Figure 9B, C). The collagen-enhancing effect of biofilm for the
455 *emm*3 strain was seen even at inocula as low as 100 CFU/well (Figure 9D), where also a dose-
456 response to collagen was evident (Figure 9D). Confocal microscopy was used to assess bacterial
457 attachment and biofilm formation with bacteria grown on glass slides with or without collagen coating.
458 In line with the crystal-violet assay, bacterial attachment of the *emm*1 (2006) and the *emm*28 (5004)
459 strain was almost completely blocked by collagen whereas the *emm*3 (2028) strain formed strong
460 robust biofilm in the presence of collagen (Figure 9E).
461

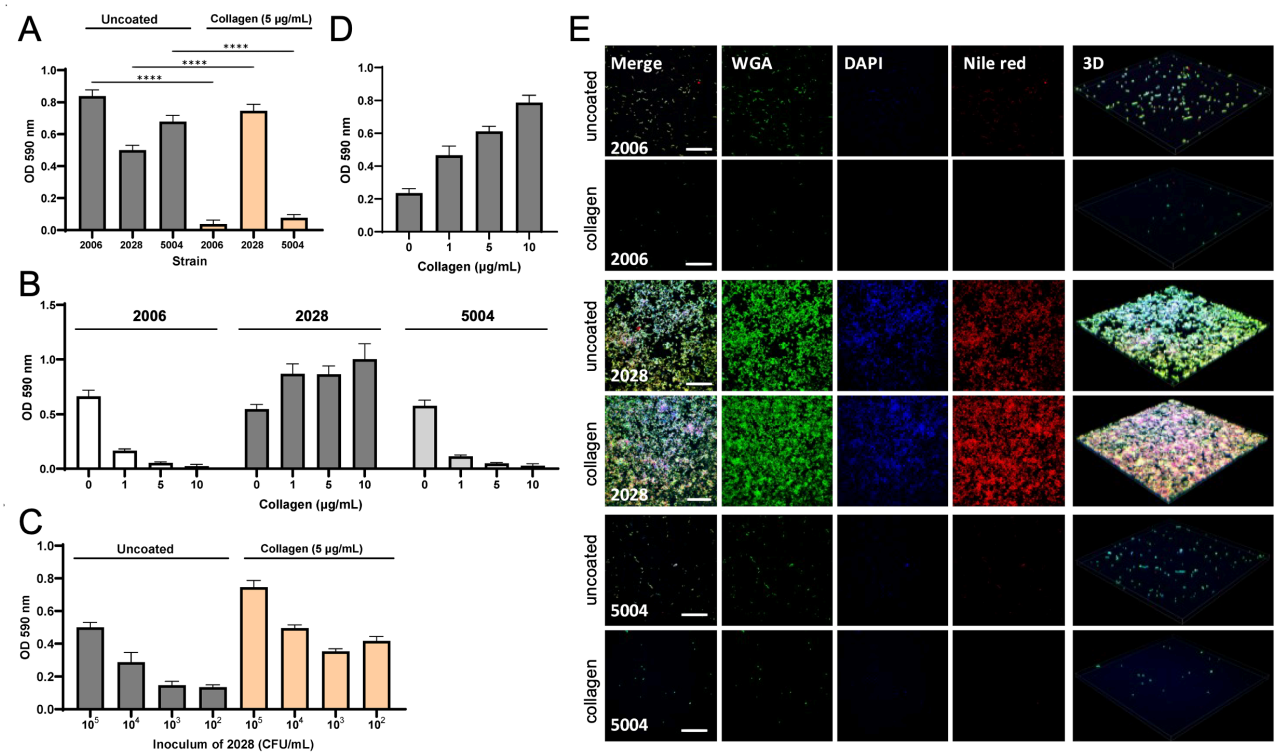

Figure 9. Effect of collagen type I on biofilm formation by necrotizing soft tissue infections strains. A) Quantitative analysis of biofilm formation on polystyrene surface with or without human type I collagen. The inoculum of each bacterial strain was 10^5 CFU per well. Significance was determined by one-way ANOVA with Tukey's *post-hoc* test. ****, P<0.0001; ***, P< 0.001; **, P< 0.01; *, P< 0.05 B) Varying effect of collagen concentration. The inoculum of each bacterial strain was 10^5 CFU per well. C) Inoculum effects on biofilm of strain 2028. D) Effect of concentration of coating collagen on strain 2028 biofilm (100 CFU per well). A-D) Results are shown as Mean + SE. All assays were repeated at least three times in triplicate. E) Confocal microscopic analysis of biofilm formation 48 h after incubation. Fluorescence staining (WGA-Alexa 488, DAPI, and Nile red) of biofilm on uncoated and collagen-coated glass slides. Scale bars indicate 50 µm.

Taken together the data shows a collagen-enhanced biofilm formation for the *emm*3, but not the *emm*1 and *emm*28 strains. To test whether this effect was linked to the M3-protein/collagen interaction, we performed competition experiments where biofilm formation of the *emm*3 (2028) strain was assessed in the presence of increasing concentrations of M3-NTD in the medium. The enhancing effect of collagen was almost completely negated in presence of 20 µM M3-NTD (Figure 10).

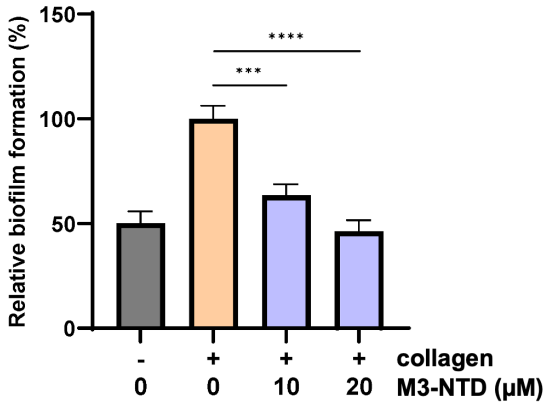

481

482 Figure 10. Competition analysis of biofilm formation of GAS isolate 2028 (100 CFU per well) in the
483 presence of M3-NTD. Results are shown as Mean + SE. All assays were repeated three times in
484 triplicate. Significance was determined by one-way ANOVA, followed by Tukey's *post-hoc* test ****,
485 P<0.0001; ***, P< 0.001.

486

487 These data indicate that the interaction between M3 protein and collagen enhances biofilm
488 formation. In further support of this finding, two additional *emm*3 strains, GAS 5626 and 8003 showed
489 a similar increase in biofilm formation on collagen-coated plates (Figure 10—figure supplement 1A).
490 The expression of M3 protein by all three *emm*3 strains was confirmed using an M3-specific antibody
491 (Figure 10—figure supplement 1B).

492

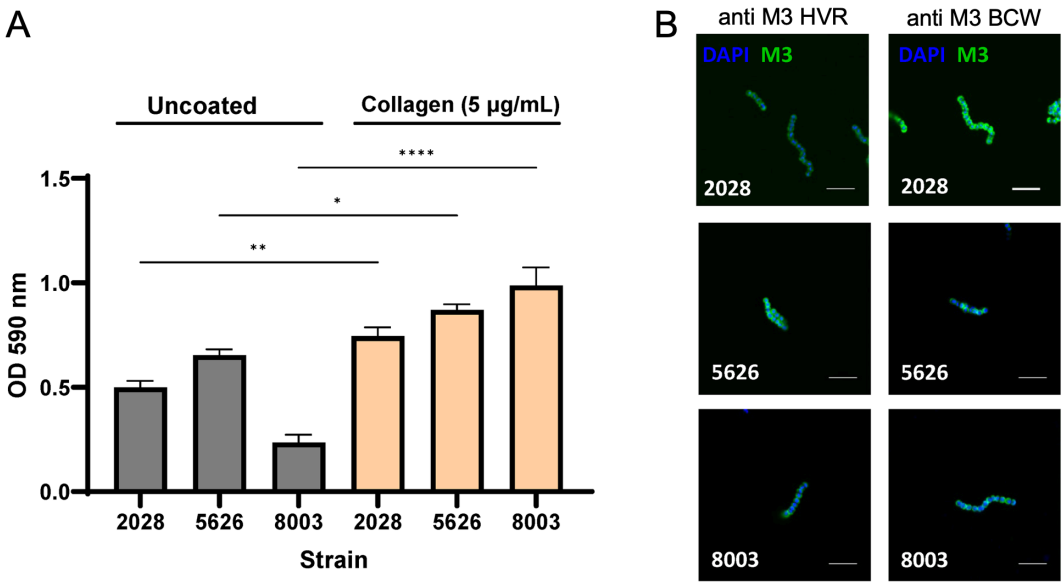

493

494

495 Figure 10—figure supplement 1. Biofilm formation of *emm*3 GAS. A) Quantitative analysis of biofilm
496 formation on polystyrene surface with or without human type I collagen. The inoculum of each
497 bacterial strain was 10^5 CFU per well. This assay was repeated at four times in triplicate and results
498 are shown as Mean + SE. Significance was determined by one-way ANOVA with Tukey's *post-hoc*

499 test. ****, P<0.0001; ***, P< 0.001; **, P< 0.01; *, P< 0.05. B) Confocal image of *emm*3 GAS stained
500 with DAPI and M3-specific antibodies. BCW, B- and C-repeat and wall-spanning regions of M3.
501 Scale bars indicate 5 μm.
502
503 ***GAS M3-collagen interaction in patient biopsies and in a 3D skin tissue model***
504 To demonstrate a potential interaction between GAS and collagen during infection, we stained tissue
505 biopsies from patients with necrotizing soft tissue infections using specific anti-GAS and anti-
506 collagen IV antibodies (Figure 11). In areas with presence of bacteria, collagen was observed to co-
507 localize with the bacteria in biopsies from two patients infected with *emm*3 strains 2028 and 5020,
508 and in one out of two patients infected with *emm*1 strains (2006 and 2068).

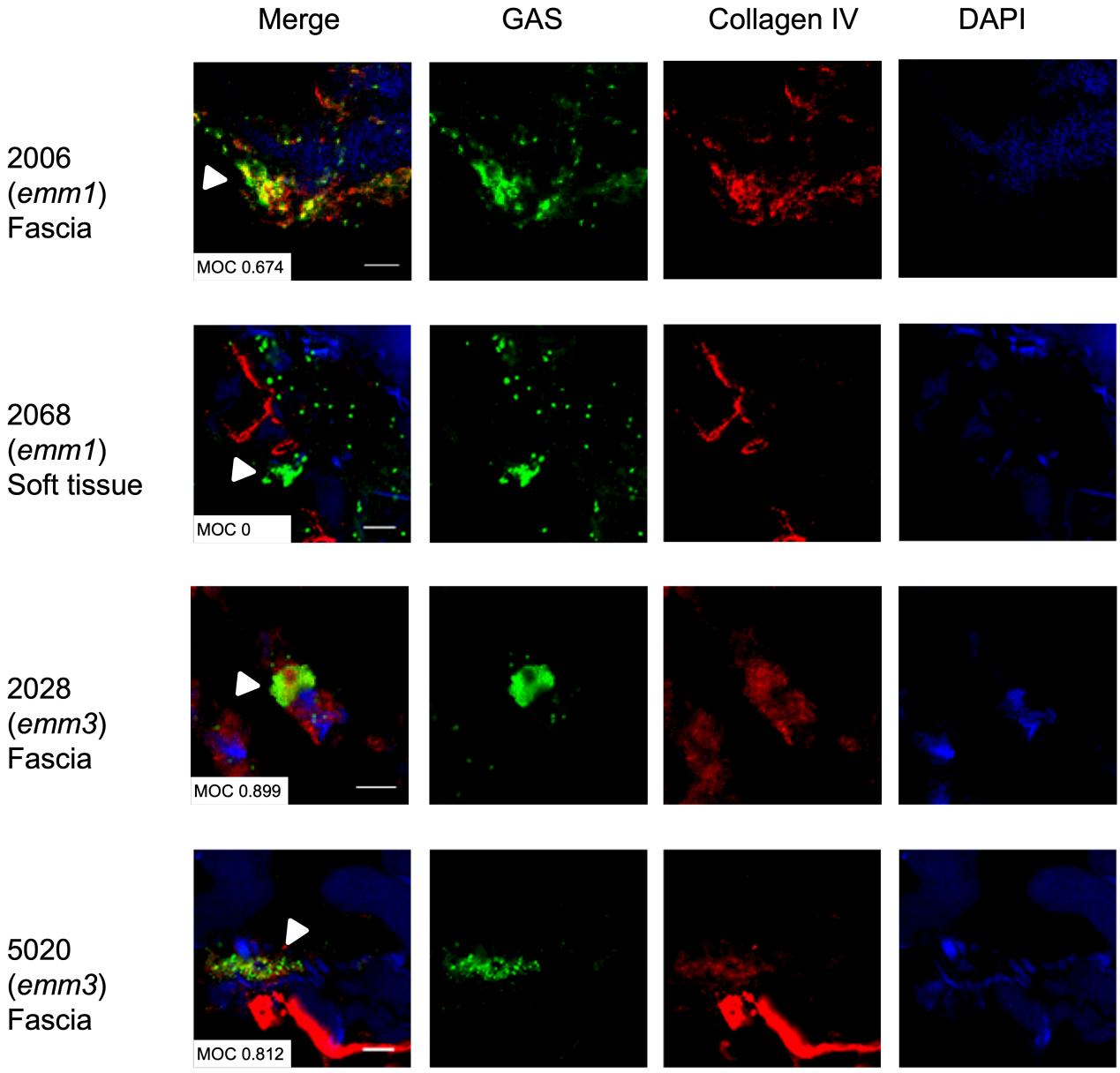

509
510 Figure 11. Colocalization of collagen with *emm3* GAS in patients' biopsies. Frozen biopsy sections
511 were stained with anti-GAS (green), anti-collagen IV (red) and DAPI (blue). Scale bars indicate 50

512 µm. The Mander's overlap coefficient (MOC) was used to quantify the colocalization of bacteria with
513 collagen.
514
515 To further investigate this in a more controlled infection model, we used a human 3D organotypic
516 skin model, which is based on a collagen type IV scaffold. We have previously employed this tissue
517 model for studies of biofilm and GAS-elicited tissue pathology [51, 52]. Infection of the skin
518 organotypic tissue with the *emm*1 (2006) and *emm*3 (2028) strains showed that both strains
519 efficiently infected the skin model tissue and caused disruption of the epithelial layer (Figure 12).
520 Bacterial load and tissue pathology increased over time, as did the colocalization of *emm*3 with
521 collagen. However, no such increase was noted in the *emm*1 strain infected models. These data
522 suggest that an interaction between *emm*3 GAS and collagen occurs in human tissue and might be
523 an important factor for biofilm formation.
524

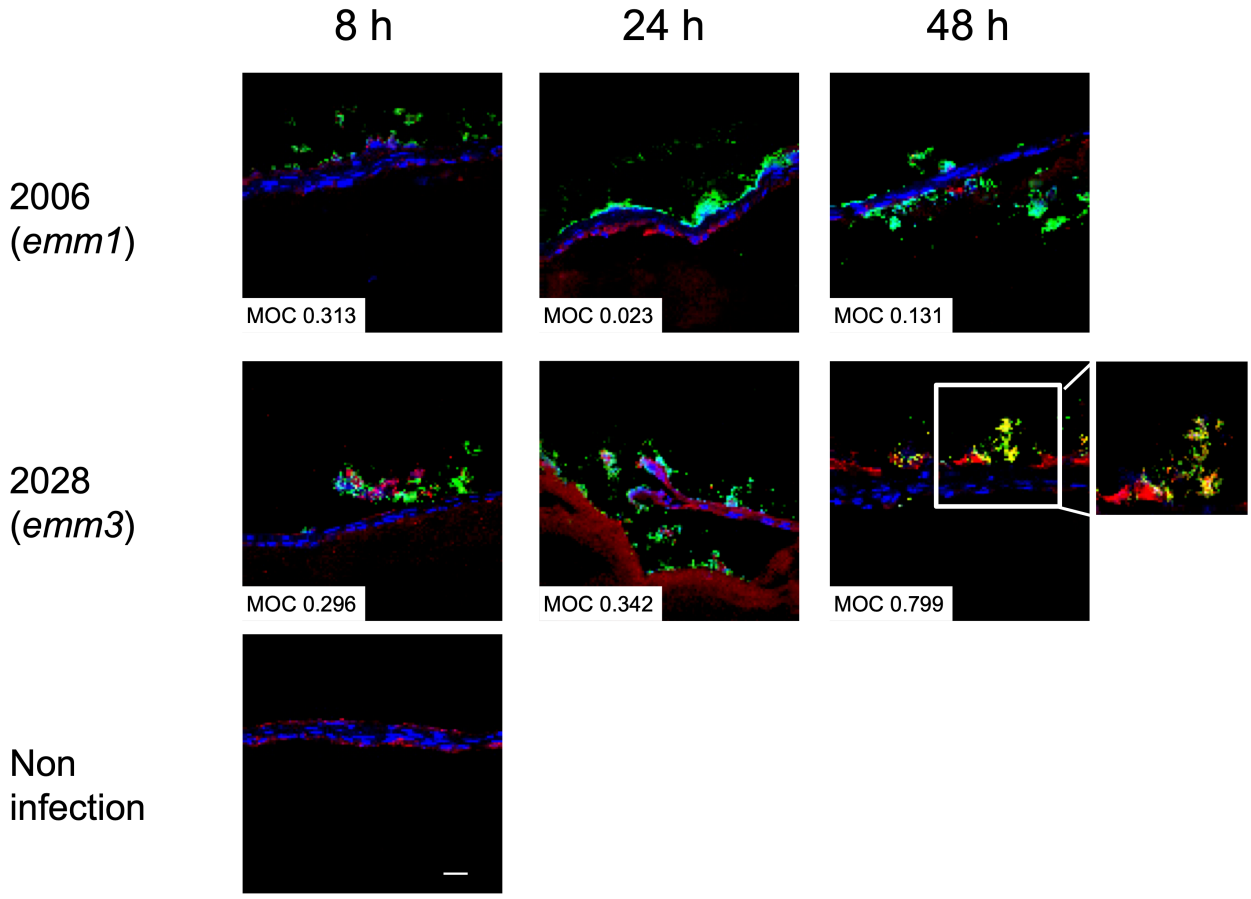

525
526 Figure 12. Colocalization of collagen with *emm3* GAS in 3D skin tissue model. Skin tissue models
527 were infected with GAS strains 2006 and 2028. At 8, 24 and 48 hours after infection, frozen sections
528 were stained with anti-GAS (green), anti-collagen IV (red) and DAPI (blue). The Mander's overlap
529 coefficient (MOC) was used to quantify the colocalization of bacteria with collagen. The merged
530 images are shown.

531
532
533 **Discussion**
534
535 No obvious or simple connection can be made between M protein sequences and the differential
536 abilities of the over 200 variants to interact with host factors. At least some activities of this major
537 streptococcal virulence factor may be encoded in hidden sequence patterns, as identified for the C4-
538 binding protein interaction with HVRs [14]. In this study, we show that the HVR of the M3 protein
539 deviates from the canonical coiled-coil structure generally assumed to be adopted by M proteins.
540 The novel T-shaped fold identified here is required for the collagen binding activity of M3. While this
541 fold may be limited to a few phylogenetically close variants of M proteins in GAS, it is more abundant
542 in SDSE. The discovery of a folded HVR may inform vaccine design. Although immunization with
543 short and therefore monomeric M protein HVR peptides may be sufficient for most GAS serotypes,
544 immunogenic epitopes of M3 may only be present in the folded, dimeric form of the protein.
545 The structures of M3-NTD alone and in presence of a collagen peptide give a rational basis for the
546 role of the PARF motif, which was previously implicated in collagen binding [33]. The role of
547 conserved residues within PARF is predominantly to stabilize the T-fold of M3-NTD. The motif alone,
548 encompassing eight residues (Ala94 to Asn101) as defined by Barroso *et al.* [32], does not present
549 all structural features involved in collagen binding based on our structure. This depends on a larger
550 region spanning residues Gln92 to Leu107 on the H2 helix, with some minor contributions of residues
551 in H1 (Figure 8). The complex structure identifies Tyr96 and Trp103 as key interface residues. They
552 provide shape complementarity and stack against proline and hydroxyproline rings of the collagen
553 triple helix. Our mutational analysis confirms a role in collagen binding for Tyr96 and Trp103.
554 Conclusions from the crystal structure are consistent with our analysis of the binding propensities of
555 the different amino acids in the CLC peptides. The observed prominent roles for hydrophobic
556 residues and for hydroxyproline in the solid-phase binding assays would be predicted from the
557 complex structure. The negative effects on binding rank of glutamate and of proline are less easy to
558 explain. Proline is restricted to the X position of the GXY triplet, which is also the position usually
559 occupied by glutamate. The effect of both residues may be to exclude more productive hydrophobic
560 amino acids from the X position. The positive role of hydroxyproline in the Y position is amply
561 demonstrated in the crystal structure. In addition to its ability to form hydrogen bonds, this may derive
562 from its greater extension from the helix axis than proline. Our findings are reminiscent of those
563 obtained for YadA [39], in that we also observed promiscuous binding to the CLC peptides, which
564 was strongly dependent on hydrophobic residues. However, in the case of YadA, the number of
565 GPO triplets and number of both Pro and Hyp also correlated with affinity.
566 The lack of specificity of CLC peptide binding and the alternative binding registers observed in the
567 crystal structure of the M3-NTD complex provide a rationale for the ability of M3 and related proteins

568 to target various types of collagens. The M3 fold recognizes the collagen triple helix through shape
569 complementarity. While collagen types differ greatly in their structural organization and biological
570 functions, their defining feature is the presence of triple-helical COL domains. The most abundant
571 collagens are the fibrillar collagens I, II, III and V, which share high sequence homology and are rich
572 in the hydrophobic and hydroxyproline residues needed to bind M3. The non-fibrillar collagens IV
573 and VI have a similar amino acid content. All these abundant collagen types contain extensive triple-
574 helical domains that we show can bind M3, and crucially, are found in the epithelial and endothelial
575 surfaces where they may encounter GAS.
576 The molecular complex described here explains how GAS of the M3 type achieve very strong binding
577 to collagens. While the affinity for the triple-helical peptides measured here by ITC is moderate, the
578 presence of two binding sites on the HVR that is found at the distal end of each M3 protein suggests
579 cooperative binding in the context of larger collagen assemblies. Most likely the bacteria do not
580 encounter isolated triple helices, but higher-order collagen structures made of bundles of triple
581 helices. It can be envisaged how M3 proteins probably intercalate between triple helices in such
582 higher-order assemblies. Given the high density of M proteins on GAS surfaces, this would generate
583 a polyvalent, high-avidity host-bacteria interface with the HVR acting as an anchor binding M3
584 perpendicularly to collagen fibrils/fibers. It is also at this higher-order structural level that an
585 explanation for the ability of M3 to induce an anti-collagen autoimmune response might be found. In
586 the rare autoimmune disease Goodpasture syndrome, an anti-collagen response is thought to be
587 caused by collagen IV neoepitopes, with infections being suggested as one possible cause for their
588 exposure [53]. It is conceivable that such neoepitopes could be generated as a result of collagen
589 structural changes caused by M3 protein binding. However, such structural rearrangements could
590 not be observed in our simplified molecular system, and our data cannot provide evidence backing
591 the anti-collagen hypothesis of post-streptococcal rheumatic sequelae [41] beyond providing the
592 molecular basis for collagen recognition by M3 protein.
593 The structural data presented here allow us to conclude that collagen binding by M proteins relies
594 on the presence of a T-shaped helical bundle domain combined with key residues to provide shape
595 complementarity to tropocollagen triple helices. But even if all GAS M protein variants included in
596 our sequence analysis bound collagens in a similar manner to M3, this would still indicate that M3-
597 like collagen binding mechanism is rare among GAS M protein variants. Based on data published
598 for M55, which was found to bind comparably weakly to collagen IV [54], it seems likely that M3 and
599 closely related serotypes have a unique ability to bind collagens in the way described here.
600 AlphaFold3 predictions support this, yielding converging structural models for the M3-collagen
601 peptide complex that closely resembled our experimental structure. This was also true for M31 and
602 M222. However, predictions with M12 and M55 resulted in low-confidence, non-converging structural
603 models with poorly defined binding sites, and/or disruption of the T-fold (Figure 6—figure supplement
604 1). On the other hand, highly confident structural predictions together with conservation of key

605 residues suggests the M3-like collagen binding mechanism is shared by SDSE and SESZ M proteins
606 (Figure 6—figure supplement 1). This has previously been experimentally validated for the FOG (or
607 Stg11) protein of SDSE, which was found to bind to collagens I and IV with high affinity [33, 42].
608 SDSE is increasingly recognized as a highly prevalent human pathogen closely resembling GAS in
609 terms of virulence traits and pathologies, including invasive infections, post-infection autoimmune
610 sequelae [35] and biofilm formation [55]. Collagen binding by M proteins may be therefore a far more
611 common virulence mechanism in human streptococcal infections than the prevalence of *emm*3 GAS
612 alone would suggest. It should be noted, too, that a new *emm*3 variant, *emm*3.93, is currently
613 emerging in the UK and the Netherlands, with a high prevalence in invasive infections [56].
614 The interaction between M protein and collagen has implications for several biological functions,
615 including bacterial attachment and biofilm formation. In this study, we investigated biofilm formation
616 due to the high prevalence of *emm*3 strains in necrotizing soft tissue infections [20], in which biofilm
617 is complicating feature [18, 57]. Our findings reveal that the M3 protein-collagen interaction promotes
618 biofilm in *emm*3 strains. Notably, for other *emm* types the presence of collagen appears to have an
619 opposing effect, reducing bacterial attachment and biofilm *in vitro* for other *emm* types. This type-
620 specific difference is further supported by observations within infected tissue models where *emm*3
621 GAS showed a more pronounced colocalization with collagen fibers, as compared to *emm*1 GAS.
622 These findings support the importance of collagen for *emm*3 biofilm development in the tissue
623 setting, while other GAS *emm* types likely utilize other mechanisms. Further studies are warranted
624 to explore the underlying mechanisms of biofilm formation in streptococcal tissue infections,
625 including not only GAS but also SDSE strains.
626
627 **Materials and Methods**
628
629 ***Cloning and site-directed mutagenesis***
630 M3-NTD DNA insert was amplified from a plasmid containing full M3 DNA sequence using primers
631 5'-GCTAGCCATGGATGCTAGGAGTGTTAATGG-3' and 5'-
632 CTAGGGATCCCTAGCAGTCCTGATATTCCTTTTC-3', digested with NcoI and BamHI and ligated
633 into the pEHISTEV vector [58], pre-digested with the same enzymes. The final M3-NTD construct,
634 after digestion with TEV protease, comprised 113 amino acids starting with Gly-Ala-Met, an artefact
635 of the purification tag. Site-directed mutagenesis was performed by PCR amplification of pEHISTEV-
636 M3NTD plasmid using mutagenic primers listed in Table 3. For selenomethionine labelling, two
637 methionine residues were introduced by substituting Ile60 and Ile141 using two sequential rounds
638 of site-directed mutagenesis.
639
640 Table 3. List of mutagenic primers.

MUTATION	PRIMER SEQUENCE (5'→3')
Tyr96Ala	GACAAAAGGCTGAAGCGCTAAAAGGCC
	GGCCTTTTAGCGCTTCAGCCTTTTGTC
Tyr96Phe	GACAAAAGGCTGAATTTCTAAAAGGCC
	GGCCTTTTAGAAATTCAGCCTTTTGTC
Trp103Ala	CCTTAATGATGCGGCTGAGAGGC
	CCTTTTAGATATTCAGCCTTTTG
Trp103Asp	CCTTAATGATGATGCTGAGAGGCTG
	CCTTTTAGATATTCAGCCTTTTG
Trp103Ile	CCTTAATGATATTGCTGAGAGGCTG
	CCTTTTAGATATTCAGCCTTTTG
Ile60Met	GTTAAATTAAAAAATGAAATGGAGAACTTGTTAGATC
	GATCTAACAAGTTCTCCATTTCATTTTTTAATTTAAC
Ile141Met	GAACTTAAGGAAAAAATGGACAAAAAGGAAAAGG
	CCTTTTCCTTTTTGTCCATTTTTTCCTTAAGTTC

641

642 ***Recombinant protein production***

643 Recombinant M3 protein was produced as an GST fusion construct as previously described [59]
644 from a pGEX6P-1 vector, a kind gift from Dr Susanne Talay, in *E. coli* BL21 (DE3) cells. The cells
645 were grown in LB media containing 100 mg/mL ampicillin at 37 ºC for 3 h after growth to an optical
646 density at 600 nm of 0.6, and induction with 1 mM isopropyl β-D-1-thiogalactopyranoside (IPTG).
647 The fusion protein was purified from bacterial cell lysate using a GSTrap 4B column according to the
648 protocol provided by the manufacturer (Cytiva). The recombinant protein comprised GST fused to a
649 proteolytic cleavage site (not used in this study) and the N-terminus of M3 (UniProt entry
650 A0A0H2UWN1), lacking N-terminal secretion signal, cell wall anchor and membrane spanning
651 region (residues 42-546).

652 M3-NTD constructs were overexpressed from pEHISTEV plasmid in *E. coli* soluBL21 cells
653 (Genlantis), in a standard LB medium supplemented with 50 mg/mL kanamycin. An overnight culture
654 was used to inoculate flasks containing 1 L of the growth medium which were incubated at 37 ºC
655 with shaking. When the optical density at 600 nm was 0.5-0.8 expression was induced by adding
656 IPTG to a final concentration of 1 mM. After 3-4 h of further incubation with shaking the cells were
657 harvested and frozen. For selenomethionine labelling the pHT-M3-NTD [Ile60Met, Ile141Met]
658 plasmid was introduced into the methionine auxotroph strain of *E. coli*, B834, which was obtained
659 from Dr Clarissa Melo Czekster. The cells from the overnight culture were washed twice with M9
660 minimal media, resuspended in 0.2x the initial volume and used to inoculate (10 mL per L) of

661 SelenoMet medium (Molecular Dimensions) supplemented with 0.04 mg/L L-selenomethionine
662 (ThermoFisher). Following induction of expression, the cells were incubated with shaking for 5 h.
663 Cell pellets were resuspended in 50-100 mL 50 mM Tris-HCl pH 8, 500 mM NaCl lysis buffer
664 supplemented with one cOmplete protease inhibitor tablet (Roche) and 1 mg DNAse I (Merck). The
665 suspension was passed twice through a Cell Disrupter (Constant Systems) at 30 kpsi and the lysate
666 was clarified by centrifugation at 20,000 x g for 25 min at 4 ºC. The supernatant was applied to a
667 HisTrap column (Cytiva) pre-equilibrated in the lysis buffer and the bound protein was washed with
668 10 column volumes of the wash buffer (50 mM Tris-HCl pH 8, 500 mM NaCl, 20 mM imidazole) and
669 eluted in a linear gradient (20-250 mM imidazole). To remove imidazole and the N-terminal
670 purification tag, the eluate was mixed with TEV protease (produced in-house) at approximately 30:1
671 stoichiometric ratio and dialyzed overnight at room temperature against phosphate-buffered saline
672 (PBS) supplemented with 1 mM dithiothreitol (DTT). The digested protein solution was passed
673 through the HisTrap column again, with PBS as the mobile phase, and M3-NTD collected in the flow-
674 through. Following concentration in 10 kDa Amicon Ultra centrifugal filters (Millipore) the protein was
675 further purified by size exclusion chromatography using Superdex75 10/300 column (Cytiva) pre-
676 equilibrated in PBS. Purity and oxidation state were verified by SDS-PAGE. If some monomeric
677 protein was still evident on the gel the fractions from size exclusion chromatography were left
678 overnight at 4 ºC. Fully oxidised protein was concentrated, aliquoted and flash frozen.
679
680 ***Collagen peptides***
681 The Collagen Ligand Collection (CLC) peptides (formerly known as Collagen Toolkits) were obtained
682 as C-terminal amides from Triple Helical Peptides Ltd, Cambridge, UK. They were synthesised on
683 TentaGel R-Ram resin using Fmoc/tBu chemistry, either on an Applied Biosystems Pioneer peptide
684 synthesiser as described previously [60], or a CEM Liberty or Liberty Blue microwave-assisted
685 peptide synthesiser. Fractions containing homogeneous product were identified by analytical HPLC
686 on an ACEphenyl300 (5 mm) column, characterised by MALDI-TOF mass spectrometry, pooled and
687 freeze-dried. In the CLCs, the variable 27-residue primary collagen structure (guest sequence) was
688 flanked by GPC$[GPP]_5$- and -$[GPP]_5$GPC (host) peptides, to ensure stable triple-helical form. In
689 JDM238, the guest sequence is GVOGEA and the host sequences $[GPO]_3$.
690
691 ***Solid phase CLC binding assay***
692 CLC peptide solid-phase binding assays were performed following a previously published protocol
693 [45, 47]. Briefly, CLC peptides, collagen II (positive control), GPP10 and bovine serum albumin (BSA)
694 (negative controls) (10 µg/mL in 0.01 M acetic acid) were immobilized on Immulon2 HB 96-well
695 plates (Nunc, Langenselbold, Germany) overnight at 4 ºC. All subsequent incubation steps were for
696 1 h at 25 ºC. The assay volume was 100 µL per well. Wells were washed three times with adhesion
697 buffer (0.1% (v/v) Tween-20 and 1 mg/mL BSA in PBS) between incubation steps. The wells were

698 blocked with 50 mg/mL BSA in PBS prior to the addition of recombinant GST-M3 at a concentration
699 of 10 µg/mL in adhesion buffer. Bound protein was detected with biotin goat anti-GST antibody
700 (Abcam) at a 1:500 dilution in adhesion buffer, followed by streptavidin-fused horseradish peroxidase
701 (HRP) and 3,3',5,5'-tetramethylbenzidine liquid substrate system (Sigma), and plates read at 450
702 nm. Including Tween in the washing steps reduced background signal but did not change the overall
703 outcome for CLC-II. It was omitted for the CLC-III assay.
704
705 ***NMR***
706 M3-NTD was isotopically labeled by expression in M9 minimal media (0.25 M Na_2HPO_4, 0.13 M
707 KH_2PO_4, 0.04 M NaCl, 18 mM $^{15}NH_4Cl$, 2.5 mM $MgSO_4$, 0.1 mM $CaCl_2$, 1% (w/v) glucose, 2.125 g/L
708 BDTM Difco™ Yeast Nitrogen Base without Amino Acids and Ammonium Sulfate (Thermo Fisher)
709 and 50 µg/mL kanamycin) and purified as described above for unlabeled protein. The NMR sample
710 contained 0.4 mM protein in 10 mM phosphate, 50 mM NaCl, pH 6.5, 1.5% (v/v) D_2O, without or with
711 addition of 10 mM DTT to generate monomeric M3-NTD. $^{1}H,^{15}N$ HSQC spectra were recorded on a
712 Bruker Ascend 700 MHz spectrometer equipped with a Prodigy TCI probe and controlled by Bruker
713 Topspin software at 30 ºC. A standard Bruker pulse sequence with gradients and water flip back
714 pulse (hsqcetfpf3gpsi) was used with 20 transients and spectral resolutions or 14.5 Hz and 41.2 Hz
715 in the direct (^{1}H) and indirect (^{15}N) dimension, respectively. Spectra were processed with NMRPipe
716 [61] and visualized with CCPN Analysis 2 [62]. For 1D 1H NMR spectra samples were prepared in
717 PBS at 0.2 mM. A standard Bruker pulse sequence with gradients and excitation sculpting for water
718 suppression (zgesgp) was used with 256 transients and a spectral resolution of 0.86 Hz. Spectra
719 were processed and visualized with Topspin.
720
721 ***Isothermal titration calorimetry***
722 Freeze-dried CLC peptides were reconstituted by dissolving in PBS (10 mg/mL), incubating the
723 solution at 75 ºC in a water bath that was left to cool slowly to room temperature overnight. M3-NTD
724 was dialysed into PBS. Experiments were performed using a MicroCal PEAQ-ITC instrument
725 (Malvern Panalytical) at 25 ºC in PBS, with the reference power set to 3 µcal/s, stirring speed to 750
726 rpm and injection speed to 0.5 µL/s. The cell contained CLC peptide at 270 µM (monomer
727 concentration) and the injector syringe contained M3-NTD variants at 1 mM (monomer
728 concentration). The only exception was the M3-NTD Trp103Ile titration, where the cell and syringe
729 solution concentrations were 165 µM and 0.61 mM, respectively. For control experiments
730 determining the heats of dilution, the cell contained PBS buffer only. Titration involved a single
731 injection of 0.4 µl followed by 18 injections of 2 µl syringe solution.
732
733 ***Protein crystallisation and structure determination***

734 Crystallization trials were conducted using the vapor diffusion sitting drop method and several sparse
735 matrix screens. M3-NTD dimer was freshly purified by size exclusion chromatography and
736 concentrated to ~700 μM (monomer concentration). For co-crystallization with JDM238 peptide, the
737 protein was concentrated to 1 mM and then diluted by adding reconstituted peptide so that the final
738 concentration of M3-NTD was 700 μM with triple-helical peptide at 1.1 mM (~1:3 ratio of M3-NTD
739 dimer to triple-helical peptide). The crystals of M3-NTD grew at 20 ºC within 1-2 weeks in 40-50% 2-
740 methyl-2,4-pentanediol (MPD), and the best one diffracted to 1.92 Å resolution. They were used for
741 streak-seeding the selenomethionine-labelled protein, which resulted in shard-like crystals diffracting
742 to 2.67 Å with the data collected at the selenium K absorption edge. Phasing of the SAD dataset
743 was conducted automatically by the Diamond Light Source (DLS) pipeline FastEP and initial model
744 building was performed using the ARP/wARP software package. The crystals of M3-NTD in complex
745 with the collagen peptide were obtained in 15% polythethylene glycol 10K, 0.1 M Tris-HCl pH 8.5,
746 0.29 M $MgSO_4$ and diffracted to 2.32 Å resolution. Indexing, scaling and merging of data was
747 performed using the autoPROC pipeline at the DLS. The complex structure was solved by molecular
748 replacement with PHASER [63] using M3-NTD and collagen peptide (PDB 3P46) structures as
749 search models, with all non-proline residues in the collagen peptide model substituted with alanine.
750 For both structures, iterative model building and refinement was performed using Coot [64] and
751 Refmac5 [65]. MolProbity [66] was used for model quality assessment. Figures of protein structure
752 models were produced using PyMOL (Schrödinger, LLC).
753
754 ***Accession codes***
755 The M3-NTD and M3-NTD/JDM238 protein structures and the data used to derive these, have been
756 deposited at the PDBe with accession codes 8p6k and 8p6j, respectively.
757
758 ***Bacterial strains***
759 GAS strains 2006 (*emm1*), 2028 (*emm3*), and 5004 (*emm28*) are isolates from patients with
760 necrotizing soft tissue infections from the INFECT project [18]. GAS 5262 and 8003 were provided
761 by Donald E. Low (Mount Sinai Hospital, Toronto, Canada) and used as further *emm3* isolates from
762 patients with necrotizing soft tissue infections [67, 68]. All isolates were cultured in either Todd-Hewitt
763 broth supplemented with 1.5% yeast extract or brain heart infusion broth at 37 ºC under a 5% CO_2
764 atmosphere.
765
766 ***Biofilm formation assay on a polystyrene surface***
767 Biofilm formation was evaluated by crystal violet staining as described previously, with minor
768 modifications [69]. Overnight cultures of the bacteria being tested were washed with PBS and diluted
769 to approximately 10^6 CFU/mL. Bacterial suspensions (100 μL) were seeded into 96-well polystyrene
770 plates (Thermo Fisher Scientific, Waltham, MA, USA). The plates were then incubated for 24 h at 37

771 ºC. After incubation, planktonic bacteria were removed by washing with PBS. Plates were then
772 stained with a 0.1% crystal violet solution (Invitrogen, Waltham, MA, USA) for 30 min. Excess crystal
773 violet was removed by washing with PBS, and then the crystal violet that was associated with
774 bacterial cells was eluted with absolute ethanol. The amount of crystal violet (and by association,
775 biofilm) was evaluated by measuring the absorbance at 590 nm using a spectrophotometer.
776 Collagen-coated plates were prepared by incubating plates with 1-10 µg/mL of collagen I overnight
777 at 4 ºC.
778
779 ***Confocal microscopic analysis of biofilm formation***
780 The biofilms were formed on an 8-well chamber slide (Lab-Tek, Thermo Fisher Scientific) in the
781 same manner as for the biofilm assay. After removing planktonic bacteria by washing with PBS, the
782 biofilms were fixed with 10% formalin and stained with wheat germ agglutinin (WGA)-Alexa Fluor
783 488 conjugate (Invitrogen) and Nile red (Invitrogen). The slides were mounted using ProLong™ Gold
784 Antifade Mountant with DAPI (Invitrogen).
785
786 ***Biofilm competition assay***
787 Recombinant M3-NTD was added at 10 and 20 µM concentrations in PBS to a collagen-coated 96-
788 well plate (0.5 µg/well) and the plate was incubated for 1 h at room temperature. After removal of
789 the protein solution, 100 µL of strain 2028 culture (ca. 10^3 CFU/mL) was seeded and incubated for
790 24 h. Biofilms were stained with crystal violet, as described above.
791
792 ***Immunofluorescent staining of GAS***
793 A few colonies were suspended in PBS on a glass slide and then fixed in 3.7% formaldehyde in PBS
794 for 15 min. The bacteria were stained with anti-M3 specific antibodies (kindly provided by Prof.
795 Gunnar Lindahl, Lund University), followed by WGA-Alexa Fluor 488 conjugate antibodies
796 (Invitrogen). The slides were mounted using ProLong™ Gold Antifade Mountant with DAPI
797 (Invitrogen).
798
799 ***Three-dimensional organotypic skin model***
800 The 3D skin models were constructed as described previously [18, 51, 52]. Briefly, 4.0×10^4 normal
801 human dermal fibroblasts (NHDF) in a collagen matrix (Pure Col, Advanced Biomatrix, Carlsbad,
802 CA, USA) were seeded onto a polymerized cell-free collagen layer in a 6-well filter insert (Corning,
803 Corning, NY, USA). After culturing in Dulbecco's Modified Eagle Medium (DMEM) for one week, 1.0
804 $\times 10^6$ human keratinocyte cells N/TERT-1 were seeded onto the NHDF layer. The models were
805 cultured in EpiLife medium (Invitrogen) for three days and exposed to air for one week. For the
806 infection assay, the models were infected with 1×10^6 CFU of bacteria for 8, 24, or 48 h.
807

808 ***Immunofluorescent staining of patient tissue biopsies and tissue models***

809 Snapfrozen tissue biopsies from patients with necrotizing soft tissue infections caused by either
810 *emm*1 GAS strains (patients 2006 and 2068) or *emm*3 GAS (patients 2028 and 5020) were available
811 from the INFECT patient biobank [18]. Cryosectioning and staining were performed as previously
812 described [52]. Briefly, the biopsies and models were embedded in an optimum cutting temperature
813 compound (Sakura, Torrance, CA, USA) and frozen in liquid nitrogen. Cryosectioning (8 µm) was
814 performed using a Leica CM3050 cryostat (Leica, Nußloch, Germany). Sections were then fixed in
815 3.7% formaldehyde in PBS for 15 min and stained with both anti-GAS (goat polyclonal antibody,
816 Abcam, Cambridge, UK) and anti-collagen IV antibodies (Abcam, Cambridge, UK), followed by
817 WGA-Alexa Fluor 488 and 546 conjugate antibodies (Invitrogen). Manders' correlation coefficient
818 was used to quantify the degree of colocalization between fluorophores and assessed with ImageJ
819 V.1.54p using the JACoP plugin V. 2.1.4. [70].

820

821 ***Statistical Analysis***

822 To compare the propensity of specific CLC amino acids to contribute to M3 binding, the A_{450} value
823 for M3 binding to BSA was subtracted from all values obtained from the solid-phase binding assays.
824 This allowed the CLC peptides to be ranked in descending order of A_{450} and divided into three
825 absorbance groups: high, from 0.75 to 0.5; medium, from 0.5 to 0.25; and low, from 0.25 to zero.
826 Data from both CLCs were pooled, and the amino acid abundance in the three groups was
827 compared. For each peptide from CLC-II and CLC-III, the number of occurrences of each amino acid
828 of interest was noted. The non-parametric Kruskal-Wallis test was used to determine whether the
829 amino acid abundance differed between the three groups. For the biofilm experiments, One-way
830 ANOVA with the Tukey's *post-hoc* test was used to determine statistically significant differences.

831

832

833 **References**

834

835 1. Brouwer S, Rivera-Hernandez T, Curren BF, Harbison-Price N, De Oliveira DMP, Jespersen
836 MG, Davies MR, Walker MJ. Pathogenesis, epidemiology and control of Group A
837 Streptococcus infection (2023) *Nature Reviews Microbiology* **21**:431-447 10.1038/s41579-
838 023-00865-7.

839 2. Carapetis JR, Steer AC, Mulholland EK, Weber M. The global burden of group A
840 streptococcal diseases (2005) *The Lancet Infectious Diseases* **5**:685-94

841 3. Jackson SJ, Steer AC, Campbell H. Systematic Review: Estimation of global burden of non-
842 suppurative sequelae of upper respiratory tract infection: rheumatic fever and post-
843 streptococcal glomerulonephritis (2011) *Tropical Medicine & International Health* **16**:2-11
844 10.1111/j.1365-3156.2010.02670.x.

845 4. Bagcchi S. Surge of invasive Group A Streptococcus disease (2023) *Lancet Infectious*
846 *Diseases* **23**:284-284 10.1016/s1473-3099(23)00043-9.

847 5. Oehmcke S, Shannon O, Morgelin M, Herwald H. Streptococcal M proteins and their role as
848 virulence determinants (2010) *Clinica Chimica Acta; International Journal of Clinical*
849 *Chemistry* **411**:1172-80 10.1016/j.cca.2010.04.032.

850 6. Smeesters PR, McMillan DJ, Sriprakash KS. The streptococcal M protein: a highly versatile
851 molecule (2010) *Trends in Microbiology* **18**:275-282 10.1016/j.tim.2010.02.007.

852 7. Walker MJ, Barnett TC, McArthur JD, Cole JN, Gillen CM, Henningham A, Sriprakash KS,
853 Sanderson-Smith ML, Nizet V. Disease manifestations and pathogenic mechanisms of
854 Group A Streptococcus (2014) *Clinical Microbiology Reviews* **27**:264-301
855 10.1128/CMR.00101-13.

856 8. Phillips GN, Jr., Flicker PF, Cohen C, Manjula BN, Fischetti VA. Streptococcal M protein:
857 alpha-helical coiled-coil structure and arrangement on the cell surface (1981) *Proceedings*
858 *of the National Academy of Sciences of the United States of America* **78**:4689-93

859 9. Nilson BHK, Frick IM, Akesson P, Forsen S, Bjorck L, Akerstrom B, Wikstrom M. Structure
860 and stability of protein-H and the M1 protein from Streptococcus-pyogenes - implications for
861 other surface-proteins of Gram-positive bacteria (1995) *Biochemistry* **34**:13688-13698
862 10.1021/bi00041a051.

863 10. Sanderson-Smith M, De Oliveira DMP, Guglielmini J, McMillan DJ, Vu T, Holien JK,
864 Henningham A, Steer AC [...], Grp MPS. A Systematic and Functional Classification of
865 *Streptococcus pyogenes* That Serves as a New Tool for Molecular Typing and Vaccine
866 Development (2014) *Journal of Infectious Diseases* **210**:1325-1338 10.1093/infdis/jiu260.

867 11. Macheboeuf P, Buffalo C, Fu CY, Zinkernagel AS, Cole JN, Johnson JE, Nizet V, Ghosh P.
868 Streptococcal M1 protein constructs a pathological host fibrinogen network (2011) *Nature*
869 **472**:64-8 10.1038/nature09967.

870 12. McNamara C, Zinkernagel AS, Macheboeuf P, Cunningham MW, Nizet V, Ghosh P. Coiled-
871 coil irregularities and instabilities in group A Streptococcus M1 are required for virulence
872 (2008) *Science* **319**:1405-8

873 13. Stewart CM, Buffalo CZ, Valderrama JA, Henningham A, Cole JN, Nizet V, Ghosh P. Coiled-
874 coil destabilizing residues in the group A Streptococcus M1 protein are required for functional
875 interaction (2016) *Proceedings of the National Academy of Sciences of the United States of*
876 *America* **113**:9515-9520 10.1073/pnas.1606160113.

877 14. Buffalo CZ, Bahn-Suh AJ, Hirakis SP, Biswas T, Amaro RE, Nizet V, Ghosh P. Conserved
878 patterns hidden within group A Streptococcus M protein hypervariability recognize human
879 C4b-binding protein (2016) *Nature Microbiology* **1** 10.1038/nmicrobiol.2016.155.

880 15. Fiedler T, Koller T, Kreikemeyer B. *Streptococcus pyogenes* biofilms-formation, biology, and
881 clinical relevance (2015) *Frontiers in Cellular and Infection Microbiology* **5**:15
882 10.3389/fcimb.2015.00015.

883 16. Hoiby N, Bjarnsholt T, Moser C, Bassi GL, Coenye T, Donelli G, Hall-Stoodley L, Hola V [...],
884 Consulting External Expert Werner Z. ESCMID guideline for the diagnosis and treatment of
885 biofilm infections 2014 (2015) *Clinical Microbiology and Infection* **21 Suppl 1**:S1-25
886 10.1016/j.cmi.2014.10.024.

887 17. Ciofu O, Moser C, Jensen PO, Hoiby N. Tolerance and resistance of microbial biofilms (2022)
888 *Nature Reviews Microbiology* **20**:621-635 10.1038/s41579-022-00682-4.

889 18. Siemens N, Chakrakodi B, Shambat SM, Morgan M, Bergsten H, Hyldegaard O, Skrede S,
890 Arnell P [...], Norrby-Teglund A. Biofilm in group A streptococcal necrotizing soft tissue
891 infections (2016) *JCI Insight* **1**:e87882 10.1172/jci.insight.87882.

892 19. Luca-Harari B, Darenberg J, Neal S, Siljander T, Strakova L, Tanna A, Creti R, Ekelund K
893 [...], Jasir A. Clinical and microbiological characteristics of severe *Streptococcus pyogenes*

894 disease in Europe (2009) *Journal of Clinical Microbiology* **47**:1155-65 10.1128/JCM.02155-
895 08.

896 20. Bruun T, Rath E, Madsen MB, Oppegaard O, Nekludov M, Arnell P, Karlsson Y, Babbar A
897 [...], Group IS. Risk Factors and Predictors of Mortality in Streptococcal Necrotizing Soft-
898 tissue Infections: A Multicenter Prospective Study (2021) *Clinical Infectious Diseases* **72**:293-
899 300 10.1093/cid/ciaa027.

900 21. Lembke C, Podbielski A, Hidalgo-Grass C, Jonas L, Hanski E, Kreikemeyer B.
901 Characterization of biofilm formation by clinically relevant serotypes of group A streptococci
902 (2006) *Applied and Environmental Microbiology* **72**:2864-75 10.1128/AEM.72.4.2864-
903 2875.2006.

904 22. Koller T, Manetti AGO, Kreikemeyer B, Lembke C, Margarit I, Grandi G, Podbielski A. Typing
905 of the pilus-protein-encoding FCT region and biofilm formation as novel parameters in
906 epidemiological investigations of *Streptococcus pyogenes* isolates from various infection
907 sites (2010) *Journal of Medical Microbiology* **59**:442-452 10.1099/jmm.0.013581-0.

908 23. Herwald H, Cramer H, Mörgelin M, Russell W, Sollenberg U, Norrby-Teglund A, Flodgaard
909 H, Lindbom L, Björck L. M protein, a classical bacterial virulence determinant, forms
910 complexes with fibrinogen that induce vascular leakage (2004) *Cell* **116**:367-379 Doi
911 10.1016/S0092-8674(04)00057-1.

912 24. Thern A, Stenberg L, Dahlback B, Lindahl G. Ig-Binding Surface-Proteins of Streptococcus-
913 Pyogenes Also Bind Human C4b-Binding Protein (C4bp), a Regulatory Component of the
914 Complement-System (1995) *Journal of Immunology* **154**:375-386

915 25. Sanderson-Smith M, Batzloff M, Sriprakash KS, Dowton M, Ranson M, Walker MJ.
916 Divergence in the plasminogen-binding group A streptococcal M protein family - Functional
917 conservation of binding site and potential role for immune selection of variants (2006) *Journal*
918 *of Biological Chemistry* **281**:3217-3226 10.1074/jbc.M508758200.

919 26. Cue D, Lam H, Cleary PP. Genetic dissection of the M1 protein: regions involved in
920 fibronectin binding and intracellular invasion (2001) *Microbial Pathogenesis* **31**:231-242 DOI
921 10.1006/mpat.2001.0467.

922 27. Dinkla K, Rohde M, Jansen WT, Kaplan EL, Chhatwal GS, Talay SR. Rheumatic fever-
923 associated *Streptococcus pyogenes* isolates aggregate collagen (2003) *Journal of Clinical*
924 *Investigation* **111**:1905-12

925 28. Bessen DE. Localization of Immunoglobulin A-Binding Sites within M or M-Like Proteins of
926 Group-A Streptococci (1994) *Infection and Immunity* **62**:1968-1974 Doi
927 10.1128/Iai.62.5.1968-1974.1994.

928 29. Quek AJH, Mazzitelli BA, Wu G, Leung EWW, Caradoc-Davies TT, Lloyd GJ, Jeevarajah D,
929 Conroy PJ [...], Law RHP. Structure and Function Characterization of the a1a2 Motifs of
930 *Streptococcus pyogenes* M Protein in Human Plasminogen Binding (2019) *Journal of*
931 *Molecular Biology* **431**:3804-3813 10.1016/j.jmb.2019.07.003.

932 30. Yuan Y, Ayinuola YA, Singh D, Ayinuola O, Mayfield JA, Quek A, Whisstock JC, Law RHP
933 [...], Castellino FJ. Solution structural model of the complex of the binding regions of human
934 plasminogen with its M-protein receptor from *Streptococcus pyogenes* (2019) *Journal of*
935 *Structural Biology* **208**:18-29 10.1016/j.jsb.2019.07.005.

936 31. Bober M, Morgelin M, Olin AI, von Pawel-Rammingen U, Collin M. The Membrane Bound
937 LRR Lipoprotein Slr, and the Cell Wall-Anchored M1 Protein from *Streptococcus pyogenes*
938 Both Interact with Type I Collagen (2011) *PLoS One* **6** 10.1371/journal.pone.0020345.

939 32. Barroso V, Rohde M, Davies MR, Gillen CM, Nitsche-Schmitz DP, Dinkla K, Chhatwal GS.
940 Identification of active variants of PARF in human pathogenic group C and group G
941 streptococci leads to an amended description of its consensus motif (2009) *International*
942 *Journal of Medical Microbiology* **299**:547-53

943 33. Dinkla K, Nitsche-Schmitz DP, Barroso V, Reissmann S, Johansson HM, Frick IM, Rohde M,
944 Chhatwal GS. Identification of a streptococcal octapeptide motif involved in acute rheumatic
945 fever (2007) *Journal of Biological Chemistry* **282**:18686-93

946 34. Brandt CM, Spellerberg B. Human Infections Due to *Streptococcus dysgalactiae* Subspecies
947 *equisimilis* (2009) *Clinical Infectious Diseases* **49**:766-772 10.1086/605085.

948 35. Xie O, Zachreson C, Tonkin-Hill G, Price DJ, Lacey JA, Morris JM, McDonald MI, Bowen AC
949 [...], Tong SYC. Overlapping *Streptococcus pyogenes* and *Streptococcus dysgalactiae*
950 subspecies *equisimilis* household transmission and mobile genetic element exchange (2024)
951 *Nature Communications* **15** 10.1038/s41467-024-47816-1.

952 36. Singh B, Fleury C, Jalalvand F, Riesbeck K. Human pathogens utilize host extracellular
953 matrix proteins laminin and collagen for adhesion and invasion of the host (2012) *FEMS*
954 *Microbiology Reviews* **36**:1122-80 10.1111/j.1574-6976.2012.00340.x.

955 37. Arora S, Gordon J, Hook M. Collagen Binding Proteins of Gram-Positive Pathogens (2021)
956 *Frontiers in Microbiology* **12** 10.3389/fmicb.2021.628798.

957 38. Zong Y, Xu Y, Liang X, Keene DR, Hook A, Gurusiddappa S, Hook M, Narayana SV. A
958 'Collagen Hug' model for Staphylococcus aureus CNA binding to collagen (2005) *EMBO*
959 *Journal* **24**:4224-36 10.1038/sj.emboj.7600888.

960 39. Leo JC, Elovaara H, Bihan D, Pugh N, Kilpinen SK, Raynal N, Skurnik M, Farndale RW,
961 Goldman A. First analysis of a bacterial collagen-binding protein with collagen Toolkits:
962 promiscuous binding of YadA to collagens may explain how YadA interferes with host
963 processes (2010) *Infection and Immunity* **78**:3226-36

964 40. van Wieringen T, Kalamajski S, Liden A, Bihan D, Guss B, Heinegard D, Farndale RW, Rubin
965 K. The streptococcal collagen-binding protein CNE specifically interferes with alphaVbeta3-
966 mediated cellular interactions with triple helical collagen (2010) *Journal of Biological*
967 *Chemistry* **285**:35803-13 10.1074/jbc.M110.146001.

968 41. Tandon R, Sharma M, Chandrashekhar Y, Kotb M, Yacoub MH, Narula J. Revisiting the
969 pathogenesis of rheumatic fever and carditis (2013) *Nature Reviews Cardiology* **10**:171-7
970 10.1038/nrcardio.2012.197.

971 42. Nitsche DP, Johansson HM, Frick IM, Mörgelin M. Streptococcal protein FOG, a novel matrix
972 adhesin interacting with collagen I *in vivo* (2006) *Journal of Biological Chemistry* **281**:1670-
973 1679 10.1074/jbc.M506776200.

974 43. Delorenzi M, Speed T. An HMM model for coiled-coil domains and a comparison with PSSM-
975 based predictions (2002) *Bioinformatics* **18**:617-25 10.1093/bioinformatics/18.4.617.

976 44. Ricard-Blum S. The Collagen Family (2011) *Cold Spring Harbor Perspectives in Biology* **3**
977 10.1101/cshperspect.a004978.

978 45. Konitsiotis AD, Raynal N, Bihan D, Hohenester E, Farndale RW, Leitinger B. Characterization
979 of high affinity binding motifs for the discoidin domain receptor DDR2 in collagen (2008)
980 *Journal of Biological Chemistry* **283**:6861-8

981 46. Zhou NE, Kay CM, Hodges RS. Disulfide bond contribution to protein stability: positional
982 effects of substitution in the hydrophobic core of the two-stranded alpha-helical coiled-coil
983 (1993) *Biochemistry* **32**:3178-87 10.1021/bi00063a033.

984 47. Howes JM, Bihan D, Slatter DA, Hamaia SW, Packman LC, Knauper V, Visse R, Farndale
985 RW. The recognition of collagen and triple-helical Toolkit peptides by MMP-13: Sequence
986 specificity for binding and cleavage (2014) *Journal of Biological Chemistry* **289**:24091-24101
987 10.1074/jbc.M114.583443.

988 48. Holm L, Laiho A, Toronen P, Salgado M. DALI shines a light on remote homologs: One
989 hundred discoveries (2023) *Protein Science* **32**:e4519 10.1002/pro.4519.

49. Abramson J, Adler J, Dunger J, Evans R, Green T, Pritzel A, Ronneberger O, Willmore L [...], Jumper JM. Accurate structure prediction of biomolecular interactions with AlphaFold 3 (2024) *Nature* **630**:493-500 10.1038/s41586-024-07487-w.

50. Hamaia SW, Pugh N, Raynal N, Nemoz B, Stone R, Gullberg D, Bihan D, Farndale RW. Mapping of potent and specific binding motifs, GLOGEN and GVOGEA, for integrin alpha1beta1 using collagen toolkits II and III (2012) *Journal of Biological Chemistry* **287**:26019-28 10.1074/jbc.M112.353144.

51. Bergsten H, Palma Medina LM, Morgan M, Moll K, Skutlaberg DH, Skrede S, Wajima T, Svensson M, Norrby-Teglund A. Adjunctive Rifampicin Increases Antibiotic Efficacy in Group A Streptococcal Tissue Infection Models (2021) *Antimicrobial Agents and Chemotherapy* **65**:e0065821 10.1128/AAC.00658-21.

52. Siemens N, Kittang BR, Chakrakodi B, Oppegaard O, Johansson L, Bruun T, Mylvaganam H, Group IS [...], Norrby-Teglund A. Increased cytotoxicity and streptolysin O activity in group G streptococcal strains causing invasive tissue infections (2015) *Scientific Reports* **5**:16945 10.1038/srep16945.

53. Pedchenko V, Kitching AR, Hudson BG. Goodpasture's autoimmune disease - A collagen IV disorder (2018) *Matrix Biology* **71-72**:240-249 10.1016/j.matbio.2018.05.004.

54. Reissmann S, Gillen CM, Fulde M, Bergmann R, Nerlich A, Rajkumari R, Brahmadathan KN, Chhatwal GS, Nitsche-Schmitz DP. Region Specific and Worldwide Distribution of Collagen-Binding M Proteins with PARF Motifs among Human Pathogenic Streptococcal Isolates (2012) *PLoS One* **7** 10.1371/journal.pone.0030122.

55. Tolken LA, Neufend JV, Oppegaard O, Methling K, Moll K, Redanz S, Katsburg MMD, Ali MQ [...], Siemens N. Streptokinase reduces Streptococcus dysgalactiae subsp. equisimilis biofilm formation (2024) *BMC Microbiology* **24**:378 10.1186/s12866-024-03540-w.

56. Davies MA, de Gier B, Guy RL, Coelho J, van Dam AP, van Houdt R, Matamoros S, van den Berg M [...], van Sorge NM. Streptococcus pyogenes emm Type 3.93 Emergence, the Netherlands and England (2025) *Emerging Infectious Diseases* **31**:229-236 10.3201/eid3102.240880.

57. Skutlaberg DH, Wiker HG, Mylvaganam H, Group IS, Norrby-Teglund A, Skrede S. Consistent Biofilm Formation by *Streptococcus pyogenes emm 1* Isolated From Patients With Necrotizing Soft Tissue Infections (2022) *Frontiers in Microbiology* **13**:822243 10.3389/fmicb.2022.822243.

58. Liu H, Naismith JH. A simple and efficient expression and purification system using two newly constructed vectors (2009) *Protein Expression and Purification* **63**:102-11 10.1016/j.pep.2008.09.008.

59. Dinkla K, Talay SR, Morgelin M, Graham RMA, Rohde M, Nitsche-Schmitz DP, Chhatwal GS. Crucial role of the CB3-region of collagen IV in PARF-induced acute rheumatic fever (2009) *PLoS One* **4**:e4666

60. Raynal N, Hamaia SW, Siljander PR, Maddox B, Peachey AR, Fernandez R, Foley LJ, Slatter DA [...], Farndale RW. Use of synthetic peptides to locate novel integrin alpha2beta1-binding motifs in human collagen III (2006) *Journal of Biological Chemistry* **281**:3821-31

61. Delaglio F, Grzesiek S, Vuister GW, Zhu G, Pfeifer J, Bax A. NMRPipe: a multidimensional spectral processing system based on UNIX pipes (1995) *Journal of Biomolecular Nmr* **6**:277-93 10.1007/BF00197809.

62. Vranken WF, Boucher W, Stevens TJ, Fogh RH, Pajon A, Llinas M, Ulrich EL, Markley JL [...], Laue ED. The CCPN data model for NMR spectroscopy: development of a software pipeline (2005) *Proteins-Structure Function and Genetics* **59**:687-96 10.1002/prot.20449.

1037 63. McCoy AJ, Grosse-Kunstleve RW, Adams PD, Winn MD, Storoni LC, Read RJ. Phaser
1038 crystallographic software (2007) *Journal of Applied Crystallography* **40**:658-674
1039 10.1107/S0021889807021206.

1040 64. Emsley P, Lohkamp B, Scott WG, Cowtan K. Features and development of Coot (2010) *Acta*
1041 *Crystallographica Section D* **66**:486-501 10.1107/S0907444910007493.

1042 65. Murshudov GN, Skubak P, Lebedev AA, Pannu NS, Steiner RA, Nicholls RA, Winn MD, Long
1043 F, Vagin AA. REFMAC5 for the refinement of macromolecular crystal structures (2011) *Acta*
1044 *Crystallographica Section D* **67**:355-67 10.1107/S0907444911001314.

1045 66. Chen VB, Arendall WB, 3rd, Headd JJ, Keedy DA, Immormino RM, Kapral GJ, Murray LW,
1046 Richardson JS, Richardson DC. MolProbity: all-atom structure validation for macromolecular
1047 crystallography (2010) *Acta Crystallographica Section D* **66**:12-21
1048 10.1107/S0907444909042073.

1049 67. Kaul R, McGeer A, Low DE, Green K, Schwartz B. Population-based surveillance for group
1050 A streptococcal necrotizing fasciitis: Clinical features, prognostic indicators, and
1051 microbiologic analysis of seventy-seven cases. Ontario Group A Streptococcal Study (1997)
1052 *American Journal of Medicine* **103**:18-24 10.1016/s0002-9343(97)00160-5.

1053 68. Johansson L, Thulin P, Sendi P, Hertzen E, Linder A, Akesson P, Low DE, Agerberth B,
1054 Norrby-Teglund A. Cathelicidin LL-37 in severe Streptococcus pyogenes soft tissue
1055 infections in humans (2008) *Infection and Immunity* **76**:3399-404 10.1128/IAI.01392-07.

1056 69. Thenmozhi R, Balaji K, Kumar R, Rao TS, Pandian SK. Characterization of biofilms in
1057 different clinical M serotypes of Streptococcus pyogenes (2011) *Journal of Basic*
1058 *Microbiology* **51**:196-204 10.1002/jobm.201000006.

1059 70. Bolte S, Cordelieres FP. A guided tour into subcellular colocalization analysis in light
1060 microscopy (2006) *J Microsc* **224**:213-32 10.1111/j.1365-2818.2006.01706.x.

1061